Article

Cell

Steroid Hormone Function Controls Non-competitive *Plasmodium* Development in *Anopheles*

Graphical Abstract

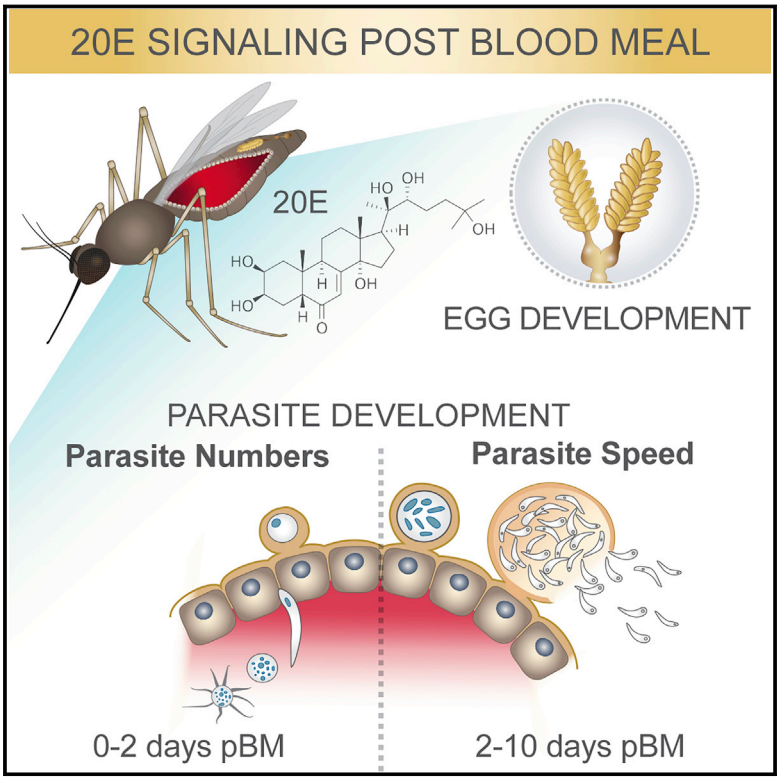

Highlights

- Human malaria parasites interact non-competitively with their mosquito vectors
- Mosquito hormone signaling co-regulates egg and parasite development
- Parasites use host lipids for their growth via a mosquito lipid transporter
- Parasites respond to mosquito metabolism with consequences for vector control

Authors

Kristine Werling, W. Robert Shaw, Maurice A. Itoe, ..., Sangeeta N. Bhatia, Clary B. Clish, Flaminia Catteruccia

Correspondence

fcatter@hsph.harvard.edu

In Brief

The development of the malaria-causing parasite *Plasmodium falciparum* depends on its ability to exploit the sexual cycle of its mosquito host in a non-competitive manner.

Werling et al., 2019, Cell *177*, 315–325
April 4, 2019
https://doi.org/10.1016/j.cell.2019.02.036

CellPress

Article

Cell

Steroid Hormone Function Controls Non-competitive *Plasmodium* Development in *Anopheles*

Kristine Werling,[1,9] W. Robert Shaw,[1,9] Maurice A. Itoe,[1,9] Kathleen A. Westervelt,[1] Perrine Marcenac,[1] Douglas G. Paton,[1] Duo Peng,[1] Naresh Singh,[1] Andrea L. Smidler,[1,2] Adam South,[1,10,11] Amy A. Deik,[3] Liliana Mancio-Silva,[4] Allison R. Demas,[4] Sandra March,[4] Eric Calvo,[5] Sangeeta N. Bhatia,[3,4,6,7,8] Clary B. Clish,[3] and Flaminia Catteruccia[1,12,*]

[1]Department of Immunology and Infectious Diseases, Harvard T.H. Chan School of Public Health, Boston, MA 02115, USA
[2]Wyss Institute for Biologically Inspired Engineering, Boston, MA 02115, USA
[3]Broad Institute, Cambridge, MA 02142, USA
[4]Institute for Medical Engineering and Science, Massachusetts Institute of Technology, Cambridge, MA 02142, USA
[5]Laboratory of Malaria and Vector Research, National Institute of Allergy and Infectious Diseases, NIH, Rockville, MD 20852, USA
[6]Howard Hughes Medical Institute, Chevy Chase, MD 20815, USA
[7]Koch Institute for Integrative Cancer Research, Cambridge, MA 02142, USA
[8]Department of Medicine, Brigham and Women's Hospital, Boston, MA 02115, USA
[9]These authors contributed equally
[10]Present address: Department of Infectious Disease and Global Health, Tufts University, Grafton, MA 01536, USA
[11]Present address: Department of Biology, Tufts University, Medford, MA 02155, USA
[12]Lead Contact
*Correspondence: fcatter@hsph.harvard.edu
https://doi.org/10.1016/j.cell.2019.02.036

SUMMARY

Transmission of malaria parasites occurs when a female *Anopheles* mosquito feeds on an infected host to acquire nutrients for egg development. How parasites are affected by oogenetic processes, principally orchestrated by the steroid hormone 20-hydroxyecdysone (20E), remains largely unknown. Here we show that *Plasmodium falciparum* development is intimately but not competitively linked to processes shaping *Anopheles gambiae* reproduction. We unveil a 20E-mediated positive correlation between egg and oocyst numbers; impairing oogenesis by multiple 20E manipulations decreases parasite intensities. These manipulations, however, accelerate *Plasmodium* growth rates, allowing sporozoites to become infectious sooner. Parasites exploit mosquito lipids for faster growth, but they do so without further affecting egg development. These results suggest that *P. falciparum* has adopted a non-competitive evolutionary strategy of resource exploitation to optimize transmission while minimizing fitness costs to its mosquito vector. Our findings have profound implications for currently proposed control strategies aimed at suppressing mosquito populations.

INTRODUCTION

Blood feeding behavior has evolved independently in multiple insect taxa as a means to acquire the necessary nutrient resources for successful reproduction. Although increasing insect reproductive fitness, the evolution of this behavior has inadvertently provided a new and effective transmission route for a multitude of human pathogens, including the mosquito-borne dengue and Zika viruses as well as *Plasmodium* parasites, the causative agents of malaria. Unquestionably, the most lethal of these pathogens is *Plasmodium falciparum*, yearly killing more than 420,000 people, mostly young African children, via the bite of highly effective anopheline species (WHO, 2018). The blood meal-triggered events that lead to egg development have been comprehensively characterized in the arboviral mosquito vector *Aedes aegypti*. In this species, blood feeding initiates the release of ovarian ecdysteroidogenic hormone (OEH) (Brown et al., 1998) and insulin-like peptides (ILPs) (Wu and Brown, 2006; Brown et al., 2008) from the brain. In turn, these factors stimulate the production of the steroid hormone ecdysone (E) from the ovarian epithelium (Brown et al., 1998; Riehle and Brown, 1999), followed by E hydroxylation to the active hormone 20E in the fat body, the mosquito fat storage organ. Upon binding to its nuclear receptor, the heterodimer ecdysone receptor (EcR)/ultraspiracle (USP), 20E triggers a vast transcriptional program that promotes the accumulation of lipids and other nutrients in the ovaries via the function of the lipid transporter *lipophorin* (*Lp*) and the yolk protein precursor *vitellogenin* (*Vg*), leading to egg development (Raikhel, 1992; Raikhel and Dhadialla, 1992; Van Heusden et al., 1997; van Heusden et al., 1998; Attardo et al., 2005). Pathways important for oogenesis appear to be largely conserved in other mosquito species, including the major malaria vector *Anopheles gambiae* (Noriega et al., 2006; Bai et al., 2010).

In *A. gambiae*, the 2- to 3-day period needed for egg development is also critical for the successful establishment of *Plasmodium* parasite infection in the midgut (Mitchell and Catteruccia, 2017). Shortly after ingestion, within the blood meal, male and female gametes fuse to form a diploid zygote that then transforms during the next 21–24 h into a motile ookinete that traverses the

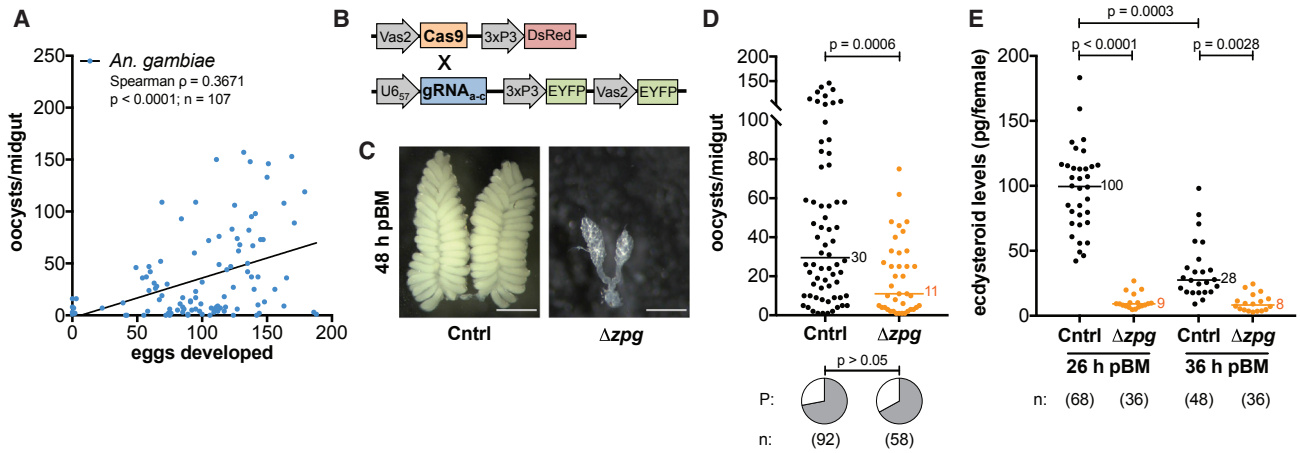

Figure 1. Parasite and Egg Development Are Linked

(A) There is a positive correlation between the number of *A. gambiae* eggs and *P. falciparum* oocysts developing in females (Spearman's correlation; line shows data trend).

(B) A transgenic *vasa2*-Cas9 mosquito line was crossed with a $U6_{57}$-Zpg gRNA transgenic line to generate Δ*zpg* mosquitoes.

(C and D) Blood-fed Δ*zpg* females (C) fail to produce eggs (scale bar, 500 μm) and (D) support fewer parasites compared with Zpg/+ controls (Cntrl) (Mann-Whitney test), whereas there is no effect on infection prevalence (P) (chi-square test).

(E) Δ*zpg* females produce lower levels of ecdysteroids 26 h and 36 h pBM (Kruskal-Wallis test, Dunn's correction).

n = sample size.

midgut epithelium before encysting beneath the midgut basal lamina and differentiating into an oocyst. During this transition, the parasite is subject to attack by the mosquito innate immune system, including lysis triggered by the complement-like thioester-containing protein TEP1 (Blandin et al., 2004; Frolet et al., 2006). After an additional 7–10 days, surviving *Plasmodium* oocysts rupture to release thousands of sporozoites that invade the salivary glands and are injected into another human host at the mosquito's next blood meal. The time from ingestion to infectivity in the mosquito is known as the parasite extrinsic incubation period (EIP), and it is a key component of malaria transmission; faster parasites have a higher chance of being transmitted, given the short lifespan of *Anopheles* females (MacDonald, 1956; Shapiro et al., 2016, 2017).

During the initial phases of infection, *Plasmodium* parasites are exposed to rapidly changing physiological conditions largely regulated by the function of ecdysteroid hormones and may be substantially affected by this blood meal-induced physiological "storm." However, whether they utilize available nutritional resources or compete for them with their mosquito hosts remains unclear. Previous work has suggested that parasites can accumulate and are affected by mosquito lipids (Atella et al., 2009; Rono et al., 2010; Costa et al., 2018), and numerous studies, albeit using unnatural vector-parasite associations, emphasize that parasites exert a fitness cost to mosquito fecundity (Hogg and Hurd, 1995; Jahan and Hurd, 1997; Ahmed et al., 1999; Ferguson et al., 2003). However, the relative fitness of parasites and mosquitoes during the course of a natural infection remains largely undetermined or difficult to interpret because of confounding factors associated with field infections (Hogg and Hurd, 1997; Sangare et al., 2014).

Here we show that development of *P. falciparum* parasites in the *A. gambiae* female is intimately linked to physiological processes modulated by 20E during egg development. By analyzing both egg and parasite numbers in individual females, we unveil an unexpected positive correlation between mosquito and parasite fitness that is dependent on 20E signaling. Although impairing oogenesis by multiple manipulations of 20E function decreases oocyst numbers, parasites respond to these metabolic changes by increasing their speed of development, becoming infectious sooner. Although faster growth depends on mosquito lipid resources via the lipid transporter Lp, it does not impair the mosquito oogenesis cycle, indicating that parasites use surplus nutrients that are not required for host reproduction. Thus, our data suggest that *P. falciparum* has adopted an evolutionary strategy that minimizes reproductive costs to its natural mosquito vector, partly explaining the formidable spread of these parasites in sub-Saharan Africa. These findings have important implications for malaria control strategies targeting mosquito reproduction.

RESULTS

P. falciparum Infections Are Linked to Egg Development in *A. gambiae*

To determine whether *Plasmodium* infections are linked to the reproductive fitness of the mosquito vector, we infected *A. gambiae* (G3 strain) females with a *P. falciparum* culture (NF54 strain) and then counted both the number of eggs developed in the ovaries and the number of oocysts present in the midgut of each individual female 8 days post-infectious blood meal (pIBM). Surprisingly, when we plotted the paired egg-parasite data and performed a correlation analysis, we found that oogenesis and intensity of infection were positively correlated (Figure 1A), demonstrating a positive link between these two processes, in contrast to the theory of vector-parasite

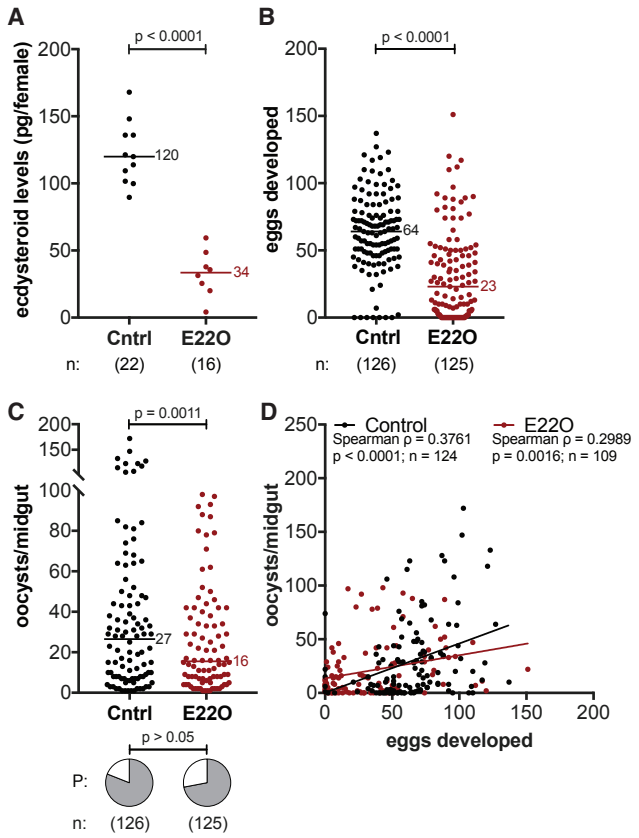

Figure 2. The Steroid Hormone 20E Regulates Both Egg and Parasite Numbers

(A) Injecting wild-type females with the ecdysteroid oxidase E22O reduces ecdysteroid levels in the female 26 h pBM compared with BSA-injected controls (Cntrl) (unpaired t test).

(B and C) E22O-injected females (B) produce fewer eggs (Mann-Whitney test) and (C) have fewer oocysts 8 days pIBM (generalized linear model [GLM], Poisson distribution). There is no effect on infection prevalence (P) (chi-square test).

(D) Egg and oocyst numbers are positively correlated in control and E22O-injected females (Spearman's correlations, lines show data trends).

n = sample size.

competition predicting costs of infection on mosquito reproduction (Schwenke et al., 2016). This correlation was observed independent of mosquito size, approximated by measuring wing length (Spearman's $\rho = 0.3224$, $n = 106$, $p = 0.0007$), and, therefore, independent of blood meal volume.

To understand the nature of the egg-parasite correlation, we next explored whether successful establishment of *P. falciparum* infection depends on the presence of fully functional ovaries. To this end, we generated transgenic *A. gambiae* females (Δ*zpg*) in which *zero population growth* (*zpg*), a gene essential for germ cell development (Tazuke et al., 2002; Thailayil et al., 2011), was mutated by CRISPR/Cas9 mutagenesis (Figure 1B). As expected, Δ*zpg* females had ablated or severely underdeveloped ovaries and largely failed to produce eggs after a blood meal (Figure 1C). When fed *P. falciparum*-infected blood, Δ*zpg* mutant females that failed to develop eggs showed significantly fewer oocysts compared with control siblings (Figure 1D), and again, this effect was independent of body size (Mann-Whitney test: oocysts ÷ wing length^3, $U = 257.5$, $p = 0.0241$). There was no difference in the prevalence of infection between the two groups (Figure 1D).

The Steroid Hormone 20E Regulates Parasite Development via Its Nuclear Receptor

The reduced oocyst load observed in Δ*zpg* mutants suggests that parasite development relies on processes that are regulated by the correct function of ovarian tissues. Given the key role of 20E in oogenesis, we went on to assess whether the function of this steroid hormone affects parasite numbers. As a first step, we determined ecdysteroid levels in Δ*zpg* mutant females 26 h and 36 h post-blood meal (pBM), around the peak of 20E synthesis (Redfern, 1982), and found severely reduced titers, as we had hypothesized, given that multiple steps of 20E synthesis occur in the ovaries (Figure 1E). To provide a direct link between 20E levels and *Plasmodium* infection, we then experimentally lowered ecdysteroid levels in *A. gambiae* by injecting wild-type females with ecdysone 22-oxidase (E22O), which oxidizes 20E (and its precursor E) in the C22 position, reducing its activity (Kamimura et al., 2012). Females injected with E22O showed a 4-fold decrease in ecdysteroid levels 26 h pBM (Figure 2A). Moreover, E22O injections prior to *P. falciparum* infection negatively affected egg development (Figure 2B) and also significantly reduced oocyst intensities, whereas the prevalence of infection remained unaffected (Figure 2C). These data provide additional evidence that 20E may regulate mosquito processes important for *P. falciparum* development.

Although E22O-injected females had limited reproductive fitness and reduced parasite loads, these females maintained a positive correlation between eggs and oocysts (Spearman's $\rho = 0.2989$, $n = 109$, $p = 0.0016$; Figure 2D). However, when we disrupted steroid hormone signaling, rather than 20E levels, by RNAi silencing of the heterodimeric nuclear receptor EcR/USP, this correlation was lost. Although we could still observe decreased egg and parasite loads in females injected with double-stranded RNA targeting *EcR* (ds*EcR*) compared with ds*GFP*-injected controls (ds*Cntrl*) (Figures 3A and 3B; STAR Methods), the number of oocysts in the midgut became unlinked from the number of eggs developed in the ovaries (Spearman's $\rho = 0.1737$, $n = 107$, $p > 0.05$; Figure 3C). We verified that 20E signaling was successfully suppressed in ds*EcR* females by detecting reduced transcripts of *Vg* (Figure 3D), which is normally induced by 20E through its nuclear receptor after blood feeding (Raikhel, 1992). Furthermore, the correlation between eggs and oocysts was also lost after silencing the 20E co-receptor *USP* (Spearman's $\rho = 0.1556$, $n = 95$, $p > 0.05$; Figure 3E), confirming that the positive interaction between mosquito and parasite fitness depends on signaling pathways controlled by 20E via its nuclear receptor.

20E Signaling Affects Early Oocyst Development in a TEP1-Independent Manner

To establish when *P. falciparum* parasite numbers are reduced following disrupted 20E signaling, we analyzed earlier developmental stages in ds*EcR* and control females by microscopy. We dissected midguts 24 h and 48 h pIBM and, after eliminating

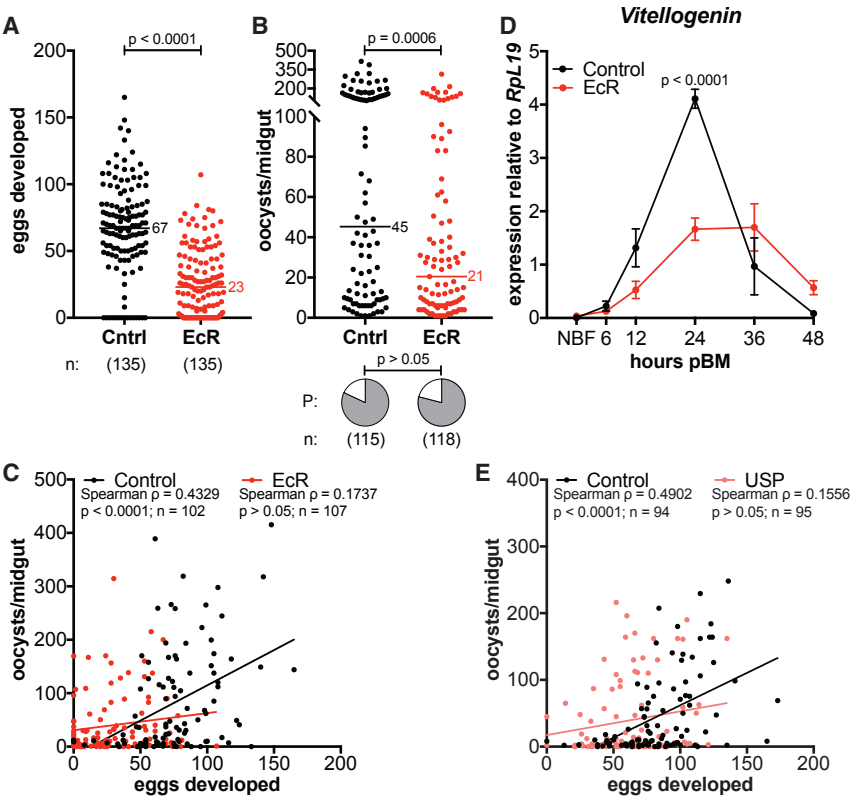

Figure 3. 20E Controls the Egg-Parasite Correlation via Its Nuclear Receptor

(A and B) Females injected with ds*EcR* (EcR) and fed a *P. falciparum*-infected blood meal (A) produce fewer eggs (Mann-Whitney test) and (B) develop fewer oocysts 7 days pIBM (GLM, Poisson distribution) compared with ds*GFP*-injected females (Cntrl). There is no effect on infection prevalence (P) (chi-square test).

(C) The positive correlation between egg and oocyst numbers is lost in ds*EcR*-injected females (Spearman's correlation).

(D) ds*EcR* females have lower *Vg* expression 24 h pBM compared with controls (means ± SEM, unpaired t test, false discovery rate [FDR]-corrected). NBF, non-blood fed.

(E) The positive egg-oocyst correlation is also lost in ds*USP*-injected females (USP) (Spearman's correlation).

n = sample size. Lines show data trends.

the blood bolus, performed immunofluorescence assays using an antibody targeting the *P. falciparum Pfs*25 surface protein to determine the number of ookinetes crossing the midgut and the number of early oocysts, respectively. Although ookinete numbers were unaffected (Figure 4A), we detected a significant reduction in early oocysts in ds*EcR* females (Figures 4B and 4C). Consistent with the lack of an observed effect on ookinete numbers, co-silencing of *TEP1*, the major immune effector that kills ookinetes during midgut invasion, did not rescue the number of oocysts in ds*EcR*/ds*TEP1* co-injected females (Figure 4D). 20E signaling, therefore, affects parasites during their transition into oocysts via TEP1-independent mechanisms.

Disrupting 20E Signaling Accelerates *P. falciparum* Growth Rates

When analyzing *Plasmodium* infections in midguts 7–8 days pIBM, we noticed that ds*EcR* females had larger oocysts than controls, which was confirmed by measuring the cross-sectional area of individual oocysts (Figures 5A and 5B). This effect was observed throughout oocyst development, as early as 5 days pIBM, the first time point when we could reliably measure parasite size. By 12 days pIBM, when some oocysts had burst to release sporozoites, there was no longer a difference between the two groups (Figure 5B). Increased size was not the result of reduced competition between parasites at lower intensities because we observed no correlation between oocyst size and numbers (ds*EcR*: Spearman's $\rho = 0.1103$, $n = 77$, $p > 0.05$; ds*GFP*: Spearman's $\rho = 0.0444$, $n = 75$, $p > 0.05$).

Larger oocysts may represent faster-developing parasites or may be the consequence of an aberrant developmental program. To address this question, we analyzed sporozoite prevalence and intensity in female salivary glands over time. Consistent with accelerated oocyst growth, sporozoites were detectable earlier and in greater numbers after perturbing 20E signaling. *EcR*-silenced females were 2.67 times more likely to have sporozoites in the glands than controls 10 days pIBM (odds ratio: 95% confidence interval [CI] = 1.13–6.25; Figure 5C), an early time point for sporozoite invasion of salivary glands. Infection intensities were also elevated in ds*EcR* females 12 days pIBM, whereas, by 14 days pIBM, the number of sporozoites was equal in both groups (Figure 5D). No difference was observed in the number of sporozoites per oocyst (Table S1), showing that the higher prevalence and intensity of infection observed in ds*EcR* females were due to accelerated growth rather than increased oocyst productivity.

Faster Parasites Are Infectious to the Vertebrate Host

Faster parasite growth could potentially occur at the expense of sporozoite fitness, causing reduced infectivity to the human host. We therefore assessed whether sporozoites collected from the salivary glands of ds*EcR* females were infectious to primary human hepatocytes, a well-established *in vitro* method to measure *P. falciparum* infectivity to humans (Mazier et al., 1985; March et al., 2013). Sporozoites dissected from ds*EcR* females 12 days pIBM were as able to invade and infect primary human hepatocytes as controls, as determined by the quantification of exoerythrocytic forms (EEFs) (Figure 5E). Consistently, we did not find any differences in sporozoite gliding motility or cell invasion, demonstrating the equivalent fitness of these faster-developing sporozoites (Figures S1A and S1B). Sporozoites from *EcR*-silenced females remained as infective as controls at later time points (18 days pIBM) (Figures S1C–S1E).

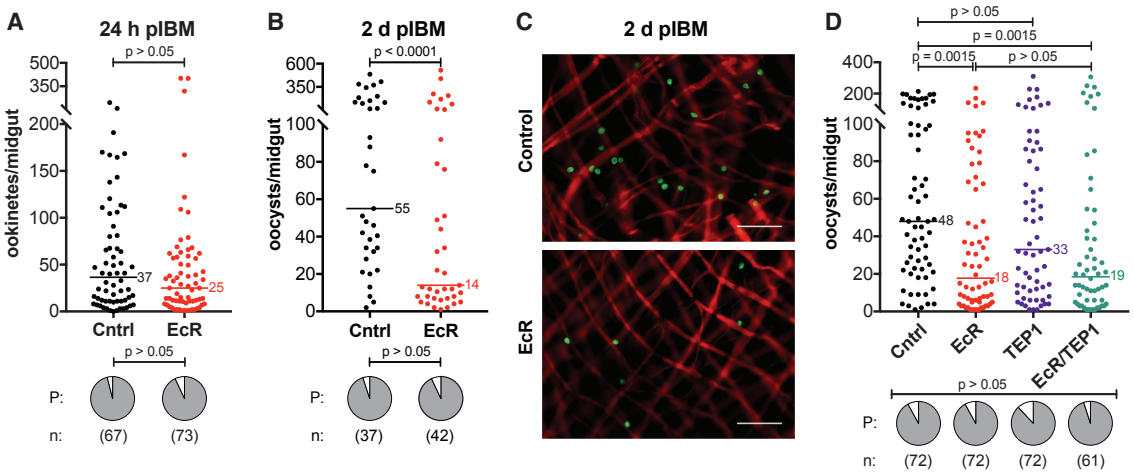

Figure 4. 20E Signaling Affects Parasites during the Ookinete-Oocyst Transition

(A) ds*EcR* injections (EcR) have no effect on the number (GLM, Poisson distribution) or prevalence (P) (Fisher's exact test) of ookinetes traversing the midgut 24 h pIBM, detected by immunofluorescent labeling of *Pfs*25 after blood bolus removal. Control, ds*GFP*-injected (Cntrl).

(B) By 2 days pIBM, ds*EcR* females have fewer oocysts compared with controls (Log(y)-transformed, GLM, normal distribution). There remains no effect on infection prevalence (P) (Fisher's exact test).

(C) Early oocysts at 2 days pIBM were detected in ds*EcR* and control midguts by *Pfs*25 (green) labeling. Red, actin (phalloidin). Scale bar, 50 μm.

(D) *TEP1* silencing does not rescue oocyst numbers in ds*EcR* females. Females injected with ds*EcR* or co-injected with ds*EcR* and ds*TEP1* (EcR/TEP1) have the same number of oocysts 7 days pIBM, and both groups have reduced oocyst numbers compared with controls. There is no effect of ds*TEP1* (TEP1) alone on oocyst numbers (Kruskal-Wallis test, Dunn's correction). Infection prevalence (P) is unaffected (Fisher's exact test).

n = sample size.

We used our prevalence data to extrapolate the length of sporogonic development in the two groups and found that the EIP_{50} (median time when 50% of mosquitoes are infectious) of *EcR*-silenced females was significantly reduced compared with controls (Figure 5F). Importantly, increased parasite growth was also detected in E22O-injected and Δ*zpg* mutant females (Figures S2A and S2B). Moreover, E22O-injected females were 2.09 times more likely than controls to have sporozoites in their salivary glands 11–12 days pIBM, similar to our observations after *EcR* silencing (odds ratio: 95% CI = 1.04–4.23; Figure S2C).

Altogether, these data demonstrate that reducing 20E function shortens the EIP of *P. falciparum* in *A. gambiae*, a trait critical for parasite transmission by the mosquito vector.

Lipid Accumulation Accelerates *P. falciparum* Growth via the Lipid Transporter Lp

What factors could be inducing faster oocyst development after 20E manipulations? Previous work determined that silencing the lipid transporter *Lp* affects oocyst size (Rono et al., 2010; Costa et al., 2018), whereas avian *Plasmodium* oocysts were found to incorporate lipids and lipid transporters in the midgut (Atella et al., 2009). We therefore examined the *Lp* expression profile of *EcR*-silenced and control females and found that although, in controls, *Lp* transcripts peaked 12 h pBM before declining (similar to findings in *Ae. aegypti*; Sun et al., 2000), in *EcR*-silenced females, the levels of *Lp* remained high up to 48 h pBM (Figure 6A). These data were confirmed by western blot using a specific antibody targeting the ApoI subunit of Lp (Figure S3A).

Because mis-regulated Lp implies altered lipid trafficking, we next determined the lipid profile of midgut tissues 24 h and 48 h pBM. ds*EcR* midguts had a significantly higher lipid content 48 h pBM (Figure 6B), a time point when early oocysts are beginning development. Specifically, four lipid species were enriched after *EcR* silencing: triacylglycerides (TAGs), diacylglycerides (DAGs), phosphatidylcholines (PCs), and lysophosphatidylethanolamines (LPEs) (Figure 6B; Figure S4A). Impairing 20E signaling thus results in a significantly altered midgut lipid profile following a blood meal.

Given the parallel increases in lipid levels and *Lp* expression in EcR-depleted females, we next assessed whether lipid trafficking by this lipid transporter was responsible for faster oocyst growth. We silenced *Lp* alone and in combination with *EcR* and analyzed egg and parasite numbers as well as oocyst size. Strikingly, co-silencing of *Lp* and *EcR* largely suppressed the increase in oocyst size observed in ds*EcR*-injected females (Figure 6C), implicating lipid species transported by this lipoprotein in parasite development. In addition, *Lp* silencing reduced egg and oocyst numbers (Figures S3B and S3C), as previously shown (Vlachou et al., 2005; Rono et al., 2010).

We next determined whether 20E levels affect the speed of parasite growth in an Lp-dependent manner also under physiological conditions. To this end, we examined whether there was a relationship between egg numbers (a proxy for 20E levels) and oocyst size (a proxy for EIP) in our control females and found a negative correlation between these parameters (Spearman's $\rho = -0.2057$, $n = 153$, $p = 0.0107$; Figure 6D). This negative correlation was, however, lost in *Lp*-silenced females, where mean oocyst size per midgut—although, in our experiments,

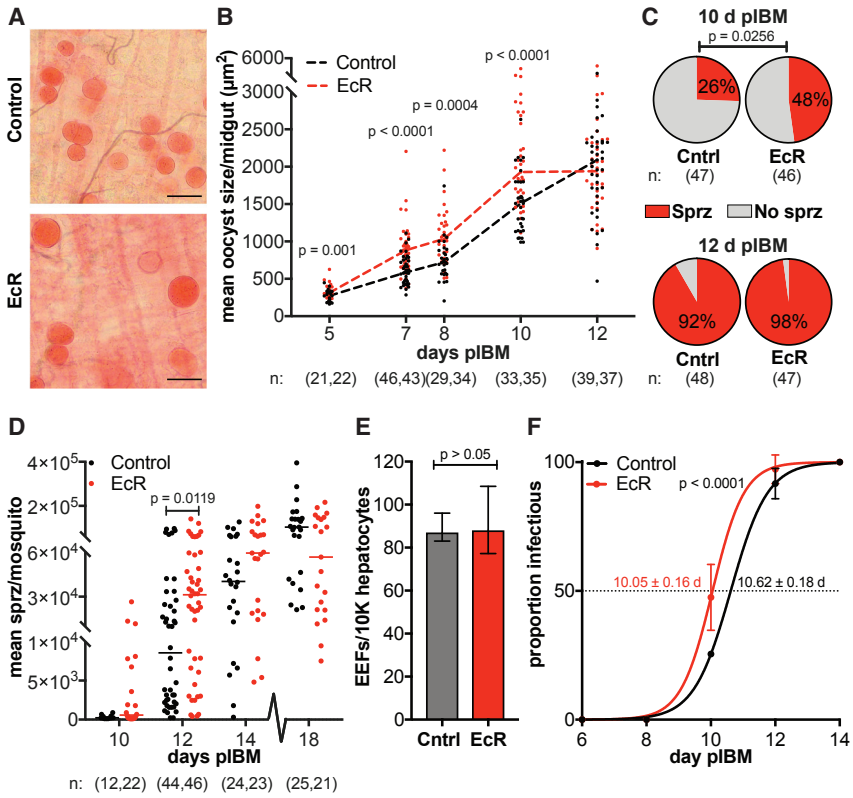

Figure 5. Disrupting 20E Signaling Promotes Faster Parasite Development

(A) Oocysts are larger in ds*EcR* females (EcR) compared with ds*GFP* (Cntrl) 8 days pIBM (scale bar, 50 μm).

(B) The mean oocyst area per midgut is higher in ds*EcR* females from 5–10 days pIBM. By 12 days pIBM, as oocysts burst, there is no difference between ds*EcR* and controls ($p > 0.05$; least-squares model).

(C and D) Salivary glands of ds*EcR* females show (C) a higher prevalence of sporozoites 10 days pIBM (chi-square test) and (D) significantly more sporozoites 12 days pIBM (Mann-Whitney test). No difference is observed at later time points (Mann-Whitney test). $p > 0.05$ where unlabeled.

(E) Salivary gland sporozoites collected from ds*EcR* females 12 days pIBM are as infectious as controls when applied to primary human hepatocytes *in vitro* (medians ± interquartile range [IQR], unpaired t test). EEF, exoerythrocytic form.

(F) The EIP_{50} (time to 50% infectious) of ds*EcR* females is significantly reduced compared with controls, as determined from the sporozoite prevalence data shown in (C) (means ± 95% CI, unpaired t test).

n = sample size with ds*GFP* listed first. See also Figures S1 and S2 and Table S1.

not significantly reduced compared with controls as in Costa et al. (2018)—was independent of egg numbers (Spearman's $\rho = 0.0404$, $n = 114$, $p > 0.05$; Figure 6D).

Altogether, these data point to 20E-regulated lipids trafficked by Lp as important factors in shaping the speed of *P. falciparum* development—the first demonstration, to our knowledge, of mosquito factors affecting the parasite EIP in the *Anopheles* female.

Faster *P. falciparum* Growth Does Not Induce a Reproductive Fitness Cost in *A. gambiae*

To rule out the possibility that, during oocyst growth, parasites deplete resources destined for egg development, we plotted the total oocyst area in individual midguts (mean oocyst area × total oocyst number) against the number of eggs in the same female and found a positive correlation between these parameters (Spearman's $\rho = 0.2837$, $n = 153$, $p = 0.0004$). This suggests parasites are not competing for resources critical for oogenesis; otherwise, we would expect their cumulative area in the midgut to be negatively correlated to the number of eggs developed.

Furthermore, we determined whether the accelerated parasite growth observed in the absence of EcR signaling occurs at the expense of egg development. To this end, we compared the number of eggs developed by *EcR*-depleted females fed either an infectious or heat-inactivated *P. falciparum* blood meal. Heat exposure renders gametocytes non-infectious while allowing females to feed on a blood meal with otherwise identical nutrition. Consistent with a lack of competition, females from both groups developed comparable numbers of eggs regardless of the presence of infectious parasites (Figure 6E).

Combined, these results point to a non-competitive strategy adopted by *P. falciparum* for optimal transmission whereby parasites exploit excess nutritional resources the *Anopheles* female does not invest toward reproduction.

Silencing the TAG Lipase *TL2* Induces Faster Parasite Growth

To establish a more direct link between lipid levels and parasite growth, we experimentally increased neutral lipids by impairing lipolysis through silencing *TAG Lipase 2* (*TL2*, *AGAP000211*). *TL2* possesses the catalytic serine residue found in the lipase active site motif (Pagni et al., 2007) and is enriched in blood-fed females (Marinotti et al., 2006). As expected, ds*TL2* injections caused an accumulation of midgut lipids, including TAGs, DAGs, and PCs (Figure 7A), as also observed by an abundance of lipid droplets in ds*TL2* midguts (Figure 7B). Three additional lipids classes were also enriched (Figure S4B). Besides raising the levels of *Lp* transcripts (Figure 7C), *TL2* silencing induced a remarkable increase in oocyst size throughout development (Figure 7D), closely phenocopying the effects observed in *EcR*-silenced females. There was no effect on the prevalence or intensity of *P. falciparum* infection (Figure S5A), and again, we observed no correlation between oocyst size and numbers, confirming a lack of competition between parasites (Spearman's $\rho = 0.1554$, $n = 37$, $p > 0.05$). Together with the *EcR*/*Lp* co-silencing results, these data further support a role for Lp-transported neutral lipids in determining parasite growth.

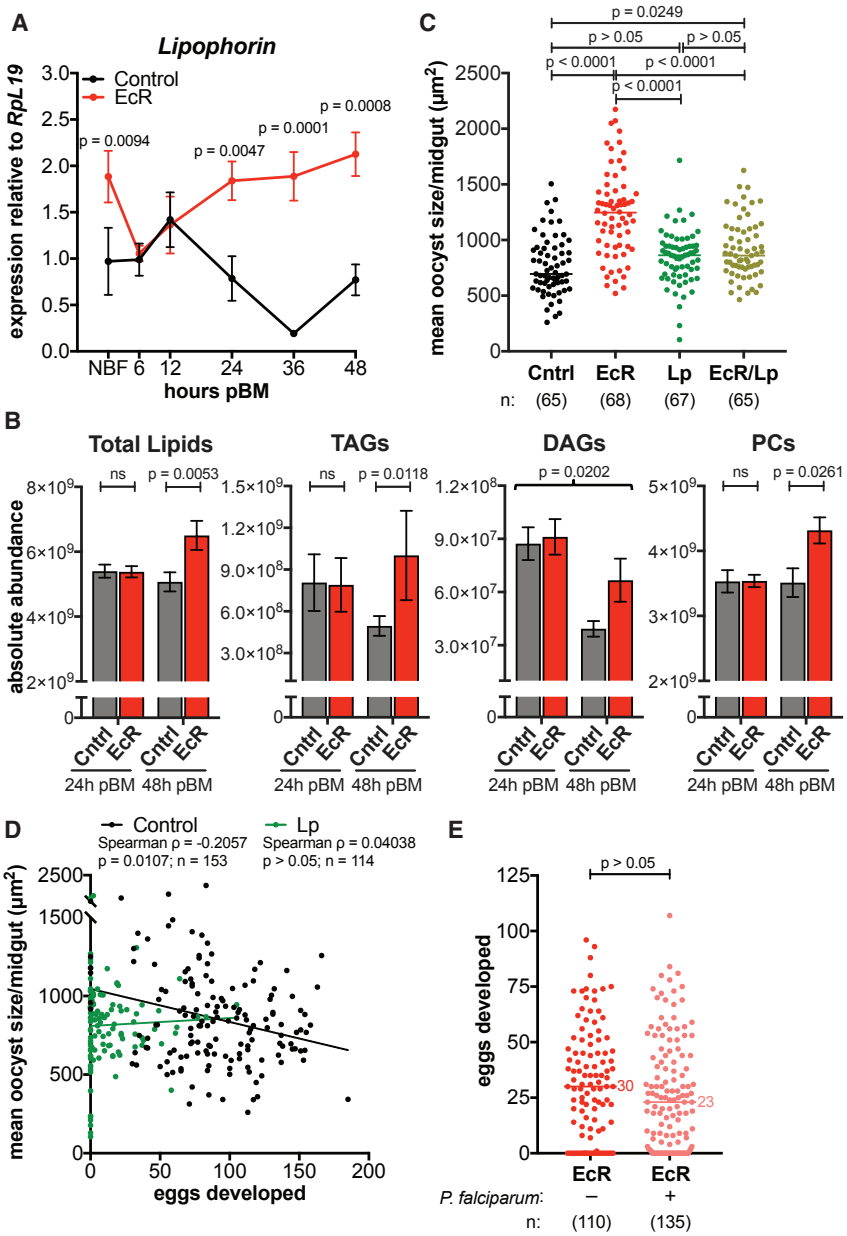

Figure 6. Faster Parasite Development Is Mediated by Lp-Transported Lipids with No Additional Cost to Fecundity

(A) *Lp* expression is elevated in ds*EcR* females (EcR) after blood feeding relative to ds*GFP* (Cntrl) (means ± SEM, unpaired t test, FDR-corrected; $p > 0.05$ where unlabeled).

(B) Total lipids, TAGs, and PCs are significantly higher in ds*EcR* midguts 48 h pIBM, whereas DAGs are increased independent of time (means ± SEM, least-squares model; ns indicates $p > 0.05$).

(C) Co-injecting females with both ds*EcR* and ds*Lp* (EcR/Lp) largely returns mean oocyst size to control levels 8 days pIBM (Kruskal-Wallis test, Dunn's correction).

(D) In ds*GFP* controls, there is a negative correlation between the number of eggs and the mean size of oocysts in individual females 8 days pIBM. This correlation is lost in ds*Lp* females (Spearman's correlations, lines show data trends).

(E) ds*EcR* females develop the same number of eggs after either an infectious or inactivated *P. falciparum* blood meal (Mann-Whitney test).

n = sample size with ds*GFP* listed first. See also Figures S3 and S4.

DISCUSSION

The parasite EIP is a key parameter of malaria transmission dynamics. Given the relatively short *Anopheles* lifespan, estimated to be around 2–3 weeks depending on species and environmental conditions (Clements and Paterson, 1981; Costantini et al., 1996), parasites with faster sporogonic development are more likely to be transmitted to the next human host (MacDonald, 1956; Shapiro et al., 2016, 2017). Despite its relevance, however, little is known about factors regulating the length of the *P. falciparum* EIP (Ohm et al., 2018). Notable exceptions are increased temperature (Paaijmans et al., 2010; Shapiro et al., 2017) and plentiful mosquito nourishment during larval stages (Shapiro et al., 2016), both associated with a shorter parasite EIP. Here we demonstrate that *P. falciparum* has the ability to respond to metabolic changes within the mosquito vector, taking advantage of resources that become available to achieve faster development without compromising sporozoite infectivity. Specifically, our data point to the 20E-dependent accumulation of glycerolipids (TAGs and DAGs) and phospholipids (PCs) in the midgut as the driver of faster, Lp-mediated parasite growth. Interestingly, in *Ae. aegypti*, which transmits several arboviruses, including dengue and Zika, inhibition of *EcR* also leads to increased TAG storage after a blood meal, possibly by downregulation of hepatocyte nuclear factor 4 (HNF4), which controls the expression of several TAG lipolytic genes (Wang et al., 2017). In our experiments, however, *EcR* silencing did not affect expression of *TL2* or other lipolytic enzymes (Figures S5B–S5D), whereas its effects were significantly reduced by co-silencing the lipid transporter *Lp*, suggesting that lipid trafficking rather than lipolysis is predominantly affected by 20E signaling. How might *P. falciparum* parasites exploit additional lipid resources to decrease EIP? The substantial growth and subdivision needed to generate thousands of sporozoites during oocyst development require significant biosynthesis of phospholipid-containing cellular membranes. Increased availability of lipids may accelerate this process in a manner similar to host lipid scavenging, which occurs during human stages of infection (Mi-Ichi et al., 2007; Itoe et al., 2014; Brancucci et al., 2017).

Disrupting egg development through *zpg* mutation, 20E inactivation, or *EcR* silencing all induced faster parasite growth, likely

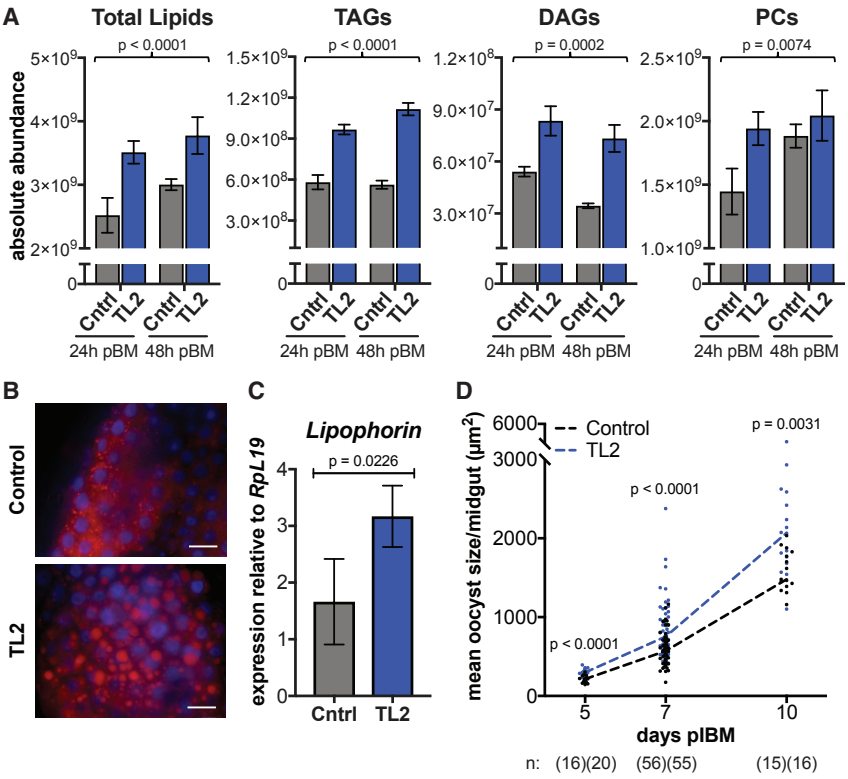

Figure 7. Silencing the TAG Lipase *TL2* Induces Faster Parasite Growth

(A) Total lipids, TAGs, DAGs, and PCs are higher in ds*TL2* midguts (TL2) 24 h and 48 h pBM compared with ds*GFP* (Cntrl) (means ± SEM, least-squares model).

(B) Midguts of ds*TL2* females stained with the neutral lipid dye LD540 (red) show an accumulation of lipid droplets 48 h pBM (scale bar, 20 μm). Blue, DAPI.

(C) *Lipophorin* expression is elevated in ds*TL2* fat bodies 24 h pBM (means ± SEM, least-squares model).

(D) ds*TL2* females develop larger oocysts from 5–10 days pIBM (Mann-Whitney test).

n = sample size with ds*GFP* listed first. See also Figures S4 and S5.

through the same metabolic mechanism (see Figure S6 for a schematic). These findings are an important warning for the deployment of mosquito population suppression methods such as gene drive systems aimed to favor the spread of factors that decrease female reproductive fitness (Burt, 2003; Hammond et al., 2016). Indeed, methods that induce changes to blood meal metabolism could lead to fewer mosquitoes that nevertheless allow faster parasite development, potentially causing an increase in *Plasmodium* transmission over a period of time. Careful assessment of interactions between pathogen development and mosquito reproductive processes is therefore essential when generating any genetically modified strain intended for field release.

Faster oocyst growth after *EcR* silencing, albeit mediated by lipid accumulation, did not further affect egg numbers. Moreover, we found no negative relationship between egg numbers and total parasite area. Based on these observations, an intriguing hypothesis is that *P. falciparum* may have followed a non-competitive evolutionary strategy based on exploiting available mosquito resources that are not needed by the female for egg development, as postulated previously (Costa et al., 2018). Reproductive costs inflicted by infection with *Plasmodium* parasites have been documented in mosquitoes, but it is worth noting that those studies used animal infection models such as *P. yoelii nigeriensis* and *P. chabaudi* (Hogg and Hurd, 1995; Jahan and Hurd, 1997; Ahmed et al., 1999; Ferguson et al., 2003), which have not coevolved with anthropophilic vectors such as *A. gambiae*. Indeed, these murine models also stimulate strong complement-mediated immune reactions (Blandin et al., 2004; Dong et al., 2006; Frolet et al., 2006) that *P. falciparum* has evolved to avoid via surface expression of *Pfs*47 (Molina-Cruz et al., 2013). One caveat of this interpretation is that we analyzed egg development after a single blood meal rather than across the entire female reproductive lifespan. Theory, however, predicts that the evolutionary costs of impairing the development of the first egg batch would be substantially larger than costs imposed during subsequent gonotrophic cycles (Koella et al., 2009). Overall, it seems plausible that a strategy of non-competitive resource exploitation during oocyst development may have favored adaptation of *P. falciparum* to *A. gambiae*, partly explaining why this mosquito-pathogen combination is so formidable at ensuring malaria transmission in sub-Saharan Africa.

The unexpected positive correlation between egg and oocyst numbers we found across a number of experiments also reinforces the notion of a non-competitive host-parasite interaction. Although we could not establish the specific mechanisms behind the reduction in parasite numbers observed after decreasing 20E titers or impairing 20E signaling, our results suggest that 20E may regulate the function of TEP1-independent immune processes targeting the early oocyst. Established theory predicts that organisms balance their energetic investment into multiple life processes at any given time because of a limited pool of available resources, often leading to reciprocal fitness trade-offs between survival, immunity, and reproduction (Schwenke et al., 2016). Our findings point to a possible regulation of these trade-offs by steroid hormones. When high 20E levels increase investment in oogenesis, a concomitant general repression of somatic or immune functions may occur, explaining how more parasites develop in females producing more eggs. In contrast, with low 20E levels, resources may be allocated preferentially toward immune or somatic processes that negatively affect parasite survival, resulting in reduced *Plasmodium* numbers, as observed in our experiments. Notably, parasite numbers were reduced during the ookinete-to-oocyst transition, which broadly corresponds to the peak of 20E synthesis. Steroid hormone

levels after blood feeding vary largely between individuals of a mosquito population (Figure 1E), likely depending on diverse factors, including larval nutritional status, microbial load, and environmental conditions as well as genetic determinants (Mamai et al., 2014). Other interpretations not involving a reproduction-immunity trade-off cannot be excluded; for instance, steroid hormone function may affect the expression of midgut components that are required for the ookinete-oocyst transition or for oocyst attachment to the basal lamina (Arrighi et al., 2005). Regardless of the mechanism, it appears that *P. falciparum* parasites have evolved their developmental strategy to respond to the mosquito reproductive investment: they either grow faster (when the female's reproductive investment is reduced), or they are more abundant (when the female invests more significantly in egg development). Moreover, they appear not to compete with each other because we see no interaction between parasite numbers and oocyst size.

Our work sheds new light on the parasite's journey within the female mosquito. By unraveling the intricate interplay between *A. gambiae* reproductive physiology and *P. falciparum* survival and growth, these studies identify the steroid hormone 20E as a major factor regulating the development of the deadliest human parasites in their most effective mosquito vectors.

STAR★METHODS

Detailed methods are provided in the online version of this paper and include the following:

- KEY RESOURCES TABLE
- CONTACT FOR REAGENT AND RESOURCE SHARING
- EXPERIMENTAL MODEL AND SUBJECT DETAILS
  - Rearing of Anopheles gambiae mosquitoes
  - Culturing of Plasmodium falciparum NF54 parasites
  - Culturing of primary human hepatocytes
- METHOD DETAILS
  - P. falciparum infections of A. gambiae mosquitoes
  - Generation of transgenic mosquito lines
  - Generation of Δzpg females
  - Ecdysteroid inactivation using the oxidase E22O
  - Measurement of ecdysteroid levels
  - Gene expression knockdown using dsRNA
  - RNA extraction, cDNA synthesis and qRT-PCR
  - Sporozoite gliding and infectivity assays
  - Western blotting
  - Staining of neutral lipids with LD540
  - Lipidomics of mosquito tissues
- QUANTIFICATION AND STATISTICAL ANALYSIS
- DATA AND SOFTWARE AVAILABILITY

SUPPLEMENTAL INFORMATION

Supplemental Information can be found with this article online at https://doi.org/10.1016/j.cell.2019.02.036.

ACKNOWLEDGMENTS

We thank Emily Lund, Casey Hill, Kate Thornburg, Sean Scott, Jamaica Siwak, and Ping Lui for help with mosquito rearing and *P. falciparum* parasite culture. We thank Evdoxia Kakani for sharing protocols, Eric Marois for the *A. gambiae* X1 and X13 lines and transgenesis plasmids, Christoph Thiele for the LD540 neutral lipid dye, Elena A. Levashina for the pLL10-Lp plasmid, Lucia Ricci for graphics support, and members of the Catteruccia laboratory for comments on the manuscript. F.C. is funded by a Faculty Research Scholar Award by the Howard Hughes Medical Institute (HHMI) and the Bill and Melinda Gates Foundation (BMGF) (Grant ID OPP1158190), and by the NIH (R01 AI124165 and R01 AI104956). A.L.S. was funded by the NIH (F31 AI120480), and P.M. was funded by a Merit/Term-Time Research Fellowship at Harvard T.H. Chan School of Public Health. Lipidomics and infection work was supported by two Broad Institute BN10 grants (to M.A.I., S.N.B., and F.C.). The findings and conclusions within this publication are those of the authors and do not necessarily reflect positions or policies of the HHMI, the BMGF, or the NIH.

AUTHOR CONTRIBUTIONS

Conceptualization, K.W., W.R.S., M.A.I., P.M., and F.C.; Methodology, K.W., W.R.S., M.A.I., and F.C.; Investigation, K.W., W.R.S., M.A.I., K.A.W., D.P., N.S., A.L.S., A.A.D., L.M.-S., A.R.D., and S.M.; Formal Analysis, K.W., W.R.S., M.A.I., D.G.P., A.S., A.A.D., L.M.-S., A.R.D., and S.M.; Writing – Original Draft, K.W., W.R.S., M.A.I., K.A.W., and F.C.; Writing – Review & Editing, K.W., W.R.S., M.A.I., K.A.W., P.M., and F.C.; Visualization, K.W., W.R.S., M.A.I., and F.C.; Funding Acquisition, W.R.S., M.A.I., P.M., A.L.S., and F.C.; Resources, E.C.; Supervision, S.N.B., C.B.C., and F.C.

DECLARATION OF INTERESTS

The authors declare no competing interests.

Received: August 16, 2018
Revised: December 14, 2018
Accepted: February 20, 2019
Published: March 28, 2019

REFERENCES

Ahmed, A.M., Maingon, R.D., Taylor, P.J., and Hurd, H. (1999). The effects of infection with Plasmodium yoelii nigeriensis on the reproductive fitness of the mosquito Anopheles gambiae. Invertebr. Reprod. Dev. *36*, 217–222.

Arrighi, R.B., Lycett, G., Mahairaki, V., Siden-Kiamos, I., and Louis, C. (2005). Laminin and the malaria parasite's journey through the mosquito midgut. J. Exp. Biol. *208*, 2497–2502.

Atella, G.C., Bittencourt-Cunha, P.R., Nunes, R.D., Shahabuddin, M., and Silva-Neto, M.A. (2009). The major insect lipoprotein is a lipid source to mosquito stages of malaria parasite. Acta Trop. *109*, 159–162.

Attardo, G.M., Hansen, I.A., and Raikhel, A.S. (2005). Nutritional regulation of vitellogenesis in mosquitoes: implications for anautogeny. Insect Biochem. Mol. Biol. *35*, 661–675.

Bai, H., Gelman, D.B., and Palli, S.R. (2010). Mode of action of methoprene in affecting female reproduction in the African malaria mosquito, Anopheles gambiae. Pest Manag. Sci. *66*, 936–943.

Baldini, F., Gabrieli, P., South, A., Valim, C., Mancini, F., and Catteruccia, F. (2013). The interaction between a sexually transferred steroid hormone and a female protein regulates oogenesis in the malaria mosquito Anopheles gambiae. PLoS Biol. *11*, e1001695.

Blandin, S., Shiao, S.H., Moita, L.F., Janse, C.J., Waters, A.P., Kafatos, F.C., and Levashina, E.A. (2004). Complement-like protein TEP1 is a determinant of vectorial capacity in the malaria vector Anopheles gambiae. Cell *116*, 661–670.

Brancucci, N.M.B., Gerdt, J.P., Wang, C., De Niz, M., Philip, N., Adapa, S.R., Zhang, M., Hitz, E., Niederwieser, I., Boltryk, S.D., et al. (2017). Lysophosphatidylcholine Regulates Sexual Stage Differentiation in the Human Malaria Parasite Plasmodium falciparum. Cell *171*, 1532–1544.e15.

Brown, M.R., Graf, R., Swiderek, K.M., Fendley, D., Stracker, T.H., Champagne, D.E., and Lea, A.O. (1998). Identification of a steroidogenic neurohormone in female mosquitoes. J. Biol. Chem. *273*, 3967–3971.

Brown, M.R., Clark, K.D., Gulia, M., Zhao, Z., Garczynski, S.F., Crim, J.W., Suderman, R.J., and Strand, M.R. (2008). An insulin-like peptide regulates egg maturation and metabolism in the mosquito Aedes aegypti. Proc. Natl. Acad. Sci. USA *105*, 5716–5721.

Burt, A. (2003). Site-specific selfish genes as tools for the control and genetic engineering of natural populations. Proc. Biol. Sci. *270*, 921–928.

Calvo, E., Mans, B.J., Andersen, J.F., and Ribeiro, J.M. (2006). Function and evolution of a mosquito salivary protein family. J. Biol. Chem. *281*, 1935–1942.

Clements, A.N., and Paterson, G.D. (1981). The analysis of mortality and survival rates in wild populations of mosquitos. J. Appl. Ecol. *18*, 373–399.

Costa, G., Gildenhard, M., Eldering, M., Lindquist, R.L., Hauser, A.E., Sauerwein, R., Goosmann, C., Brinkmann, V., Carrillo-Bustamante, P., and Levashina, E.A. (2018). Non-competitive resource exploitation within mosquito shapes within-host malaria infectivity and virulence. Nat. Commun. *9*, 3474.

Costantini, C., Li, S.G., Della Torre, A., Sagnon, N., Coluzzi, M., and Taylor, C.E. (1996). Density, survival and dispersal of Anopheles gambiae complex mosquitoes in a west African Sudan savanna village. Med. Vet. Entomol. *10*, 203–219.

Doench, J.G., Fusi, N., Sullender, M., Hegde, M., Vaimberg, E.W., Donovan, K.F., Smith, I., Tothova, Z., Wilen, C., Orchard, R., et al. (2016). Optimized sgRNA design to maximize activity and minimize off-target effects of CRISPR-Cas9. Nat. Biotechnol. *34*, 184–191.

Dong, Y., Aguilar, R., Xi, Z., Warr, E., Mongin, E., and Dimopoulos, G. (2006). Anopheles gambiae immune responses to human and rodent Plasmodium parasite species. PLoS Pathog. *2*, e52.

Ferguson, H.M., Rivero, A., and Read, A.F. (2003). The influence of malaria parasite genetic diversity and anaemia on mosquito feeding and fecundity. Parasitology *127*, 9–19.

Frolet, C., Thoma, M., Blandin, S., Hoffmann, J.A., and Levashina, E.A. (2006). Boosting NF-kappaB-dependent basal immunity of Anopheles gambiae aborts development of Plasmodium berghei. Immunity *25*, 677–685.

Gibbons, J.G., Janson, E.M., Hittinger, C.T., Johnston, M., Abbot, P., and Rokas, A. (2009). Benchmarking next-generation transcriptome sequencing for functional and evolutionary genomics. Mol. Biol. Evol. *26*, 2731–2744.

Hammond, A., Galizi, R., Kyrou, K., Simoni, A., Siniscalchi, C., Katsanos, D., Gribble, M., Baker, D., Marois, E., Russell, S., et al. (2016). A CRISPR-Cas9 gene drive system targeting female reproduction in the malaria mosquito vector Anopheles gambiae. Nat. Biotechnol. *34*, 78–83.

Hansen, I.A., Attardo, G.M., Roy, S.G., and Raikhel, A.S. (2005). Target of rapamycin-dependent activation of S6 kinase is a central step in the transduction of nutritional signals during egg development in a mosquito. J. Biol. Chem. *280*, 20565–20572.

Hofacker, I.L., Fontana, W., Stadler, P.F., Bonhoeffer, L.S., Tacker, M., and Schuster, P. (1994). Fast folding and comparison of RNA secondary structures. Monatsh. Chem. *125*, 167–188.

Hogg, J.C., and Hurd, H. (1995). Plasmodium yoelii nigeriensis: the effect of high and low intensity of infection upon the egg production and bloodmeal size of Anopheles stephensi during three gonotrophic cycles. Parasitology *111*, 555–562.

Hogg, J.C., and Hurd, H. (1997). The effects of natural Plasmodium falciparum infection on the fecundity and mortality of Anopheles gambiae s. l. in north east Tanzania. Parasitology *114*, 325–331.

Hsu, P.D., Scott, D.A., Weinstein, J.A., Ran, F.A., Konermann, S., Agarwala, V., Li, Y., Fine, E.J., Wu, X., Shalem, O., et al. (2013). DNA targeting specificity of RNA-guided Cas9 nucleases. Nat. Biotechnol. *31*, 827–832.

Ifediba, T., and Vanderberg, J.P. (1981). Complete in vitro maturation of Plasmodium falciparum gametocytes. Nature *294*, 364–366.

Itoe, M.A., Sampaio, J.L., Cabal, G.G., Real, E., Zuzarte-Luis, V., March, S., Bhatia, S.N., Frischknecht, F., Thiele, C., Shevchenko, A., and Mota, M.M. (2014). Host cell phosphatidylcholine is a key mediator of malaria parasite survival during liver stage infection. Cell Host Microbe *16*, 778–786.

Jahan, N., and Hurd, H. (1997). The effects of infection with Plasmodium yoelii nigeriensis on the reproductive fitness of Anopheles stephensi. Ann. Trop. Med. Parasitol. *91*, 365–369.

Jaramillo-Gutierrez, G., Rodrigues, J., Ndikuyeze, G., Povelones, M., Molina-Cruz, A., and Barillas-Mury, C. (2009). Mosquito immune responses and compatibility between Plasmodium parasites and anopheline mosquitoes. BMC Microbiol. *9*, 154.

Kamimura, M., Saito, H., Niwa, R., Niimi, T., Toyoda, K., Ueno, C., Kanamori, Y., Shimura, S., and Kiuchi, M. (2012). Fungal ecdysteroid-22-oxidase, a new tool for manipulating ecdysteroid signaling and insect development. J. Biol. Chem. *287*, 16488–16498.

Koella, J.C., Lynch, P.A., Thomas, M.B., and Read, A.F. (2009). Towards evolution-proof malaria control with insecticides. Evol. Appl. *2*, 469–480.

MacDonald, G. (1956). Epidemiological basis of malaria control. Bull. World Health Organ. *15*, 613–626.

Mamai, W., Mouline, K., Blais, C., Larvor, V., Dabiré, K.R., Ouedraogo, G.A., Simard, F., and Renault, D. (2014). Metabolomic and ecdysteroid variations in Anopheles gambiae s.l. mosquitoes exposed to the stressful conditions of the dry season in Burkina Faso, West Africa. Physiol. Biochem. Zool. *87*, 486–497.

March, S., Ng, S., Velmurugan, S., Galstian, A., Shan, J., Logan, D.J., Carpenter, A.E., Thomas, D., Sim, B.K., Mota, M.M., et al. (2013). A microscale human liver platform that supports the hepatic stages of Plasmodium falciparum and vivax. Cell Host Microbe *14*, 104–115.

March, S., Ramanan, V., Trehan, K., Ng, S., Galstian, A., Gural, N., Scull, M.A., Shlomai, A., Mota, M.M., Fleming, H.E., et al. (2015). Micropatterned coculture of primary human hepatocytes and supportive cells for the study of hepatotropic pathogens. Nat. Protoc. *10*, 2027–2053.

Marinotti, O., Calvo, E., Nguyen, Q.K., Dissanayake, S., Ribeiro, J.M., and James, A.A. (2006). Genome-wide analysis of gene expression in adult Anopheles gambiae. Insect Mol. Biol. *15*, 1–12.

Mazier, D., Beaudoin, R.L., Mellouk, S., Druilhe, P., Texier, B., Trosper, J., Miltgen, F., Landau, I., Paul, C., Brandicourt, O., et al. (1985). Complete development of hepatic stages of Plasmodium falciparum in vitro. Science *227*, 440–442.

Mi-Ichi, F., Kano, S., and Mitamura, T. (2007). Oleic acid is indispensable for intraerythrocytic proliferation of Plasmodium falciparum. Parasitology *134*, 1671–1677.

Mitchell, S.N., and Catteruccia, F. (2017). Anopheline Reproductive Biology: Impacts on Vectorial Capacity and Potential Avenues for Malaria Control. Cold Spring Harb. Perspect. Med. *7*, a025593.

Molina-Cruz, A., Garver, L.S., Alabaster, A., Bangiolo, L., Haile, A., Winikor, J., Ortega, C., van Schaijk, B.C., Sauerwein, R.W., Taylor-Salmon, E., and Barillas-Mury, C. (2013). The human malaria parasite Pfs47 gene mediates evasion of the mosquito immune system. Science *340*, 984–987.

Noriega, F.G., Ribeiro, J.M., Koener, J.F., Valenzuela, J.G., Hernandez-Martinez, S., Pham, V.M., and Feyereisen, R. (2006). Comparative genomics of insect juvenile hormone biosynthesis. Insect Biochem. Mol. Biol. *36*, 366–374.

Ohm, J.R., Baldini, F., Barreaux, P., Lefevre, T., Lynch, P.A., Suh, E., Whitehead, S.A., and Thomas, M.B. (2018). Rethinking the extrinsic incubation period of malaria parasites. Parasit. Vectors *11*, 178.

Paaijmans, K.P., Blanford, S., Bell, A.S., Blanford, J.I., Read, A.F., and Thomas, M.B. (2010). Influence of climate on malaria transmission depends on daily temperature variation. Proc. Natl. Acad. Sci. USA *107*, 15135–15139.

Pagni, M., Ioannidis, V., Cerutti, L., Zahn-Zabal, M., Jongeneel, C.V., Hau, J., Martin, O., Kuznetsov, D., and Falquet, L. (2007). MyHits: improvements to an interactive resource for analyzing protein sequences. Nucleic Acids Res. *35*, W433–W437.

Papathanos, P.A., Windbichler, N., Menichelli, M., Burt, A., and Crisanti, A. (2009). The vasa regulatory region mediates germline expression and maternal

transmission of proteins in the malaria mosquito Anopheles gambiae: a versatile tool for genetic control strategies. BMC Mol. Biol. *10*, 65.

Raikhel, A.S. (1992). Vitellogenesis in mosquitoes. In Advances in Disease Vector Research, K.F. Harris, ed. (Springer), pp. 1–39.

Raikhel, A.S., and Dhadialla, T.S. (1992). Accumulation of yolk proteins in insect oocytes. Annu. Rev. Entomol. *37*, 217–251.

Ran, F.A., Hsu, P.D., Wright, J., Agarwala, V., Scott, D.A., and Zhang, F. (2013). Genome engineering using the CRISPR-Cas9 system. Nat. Protoc. *8*, 2281–2308.

Redfern, C.P.F. (1982). 20-Hydroxy-ecdysone and ovarian development in Anopheles stephensi. J. Insect Physiol. *28*, 97–109.

Rheinwald, J.G., and Green, H. (1975). Serial cultivation of strains of human epidermal keratinocytes: the formation of keratinizing colonies from single cells. Cell *6*, 331–343.

Riehle, M.A., and Brown, M.R. (1999). Insulin stimulates ecdysteroid production through a conserved signaling cascade in the mosquito Aedes aegypti. Insect Biochem. Mol. Biol. *29*, 855–860.

Rogers, D.W., Whitten, M.M.A., Thailayil, J., Soichot, J., Levashina, E.A., and Catteruccia, F. (2008). Molecular and cellular components of the mating machinery in Anopheles gambiae females. Proc. Natl. Acad. Sci. USA *105*, 19390–19395.

Rogers, D.W., Baldini, F., Battaglia, F., Panico, M., Dell, A., Morris, H.R., and Catteruccia, F. (2009). Transglutaminase-mediated semen coagulation controls sperm storage in the malaria mosquito. PLoS Biol. *7*, e1000272.

Rono, M.K., Whitten, M.M., Oulad-Abdelghani, M., Levashina, E.A., and Marois, E. (2010). The major yolk protein vitellogenin interferes with the anti-plasmodium response in the malaria mosquito Anopheles gambiae. PLoS Biol. *8*, e1000434.

Sangare, I., Dabire, R., Yameogo, B., Da, D.F., Michalakis, Y., and Cohuet, A. (2014). Stress dependent infection cost of the human malaria agent Plasmodium falciparum on its natural vector Anopheles coluzzii. Infect. Genet. Evol. *25*, 57–65.

Santolamazza, F., Mancini, E., Simard, F., Qi, Y., Tu, Z., and della Torre, A. (2008). Insertion polymorphisms of SINE200 retrotransposons within speciation islands of Anopheles gambiae molecular forms. Malar. J. *7*, 163.

Schindelin, J., Arganda-Carreras, I., Frise, E., Kaynig, V., Longair, M., Pietzsch, T., Preibisch, S., Rueden, C., Saalfeld, S., Schmid, B., et al. (2012). Fiji: an open-source platform for biological-image analysis. Nat. Methods *9*, 676–682.

Schwenke, R.A., Lazzaro, B.P., and Wolfner, M.F. (2016). Reproduction-Immunity Trade-Offs in Insects. Annu. Rev. Entomol. *61*, 239–256.

Shapiro, L.L., Murdock, C.C., Jacobs, G.R., Thomas, R.J., and Thomas, M.B. (2016). Larval food quantity affects the capacity of adult mosquitoes to transmit human malaria. Proc. Biol. Sci. *283*, 20160298.

Shapiro, L.L.M., Whitehead, S.A., and Thomas, M.B. (2017). Quantifying the effects of temperature on mosquito and parasite traits that determine the transmission potential of human malaria. PLoS Biol. *15*, e2003489.

Snounou, G., Viriyakosol, S., Zhu, X.P., Jarra, W., Pinheiro, L., do Rosario, V.E., Thaithong, S., and Brown, K.N. (1993). High sensitivity of detection of human malaria parasites by the use of nested polymerase chain reaction. Mol. Biochem. Parasitol. *61*, 315–320.

Spandl, J., White, D.J., Peychl, J., and Thiele, C. (2009). Live cell multicolor imaging of lipid droplets with a new dye, LD540. Traffic *10*, 1579–1584.

Sun, J., Hiraoka, T., Dittmer, N.T., Cho, K.-H., and Raikhel, A.S. (2000). Lipophorin as a yolk protein precursor in the mosquito, Aedes aegypti. Insect Biochem. Mol. Biol. *30*, 1161–1171.

Tazuke, S.I., Schulz, C., Gilboa, L., Fogarty, M., Mahowald, A.P., Guichet, A., Ephrussi, A., Wood, C.G., Lehmann, R., and Fuller, M.T. (2002). A germline-specific gap junction protein required for survival of differentiating early germ cells. Development *129*, 2529–2539.

Thailayil, J., Magnusson, K., Godfray, H.C.J., Crisanti, A., and Catteruccia, F. (2011). Spermless males elicit large-scale female responses to mating in the malaria mosquito Anopheles gambiae. Proc. Natl. Acad. Sci. USA *108*, 13677–13681.

Trager, W., and Jensen, J.B. (1976). Human malaria parasites in continuous culture. Science *193*, 673–675.

Tsuji, M., Mattei, D., Nussenzweig, R.S., Eichinger, D., and Zavala, F. (1994). Demonstration of heat-shock protein 70 in the sporozoite stage of malaria parasites. Parasitol. Res. *80*, 16–21.

Van Heusden, M.C., Erickson, B.A., and Pennington, J.E. (1997). Lipophorin levels in the yellow fever mosquito, Aedes aegypti, and the effect of feeding. Arch. Insect Biochem. Physiol. *34*, 301–312.

van Heusden, M.C., Thompson, F., and Dennis, J. (1998). Biosynthesis of Aedes aegypti lipophorin and gene expression of its apolipoproteins. Insect Biochem. Mol. Biol. *28*, 733–738.

Vlachou, D., Schlegelmilch, T., Christophides, G.K., and Kafatos, F.C. (2005). Functional genomic analysis of midgut epithelial responses in Anopheles during Plasmodium invasion. Curr. Biol. *15*, 1185–1195.

Volohonsky, G., Terenzi, O., Soichot, J., Naujoks, D.A., Nolan, T., Windbichler, N., Kapps, D., Smidler, A.L., Vittu, A., Costa, G., et al. (2015). Tools for Anopheles gambiae Transgenesis. G3 (Bethesda) *5*, 1151–1163.

Wang, X., Hou, Y., Saha, T.T., Pei, G., Raikhel, A.S., and Zou, Z. (2017). Hormone and receptor interplay in the regulation of mosquito lipid metabolism. Proc. Natl. Acad. Sci. USA *114*, E2709–E2718.

WHO (2018). World Malaria Report (World Health Organization).

Wu, Q., and Brown, M.R. (2006). Signaling and function of insulin-like peptides in insects. Annu. Rev. Entomol. *51*, 1–24.

Ye, J., Coulouris, G., Zaretskaya, I., Cutcutache, I., Rozen, S., and Madden, T.L. (2012). Primer-BLAST: a tool to design target-specific primers for polymerase chain reaction. BMC Bioinformatics *13*, 134.

STAR★METHODS

KEY RESOURCES TABLE

REAGENT or RESOURCE	SOURCE	IDENTIFIER
Antibodies		
Mouse monoclonal αPfs25 (clone 4B7)	B.E.I. Resources	Cat#MRA-28; RRID: AB_2728658
Mouse monoclonal αPfCSP (clone 2A10)	B.E.I. Resources	Cat#MRA-183A
Mouse monoclonal αPfHSP70 (clone 4C9)	F. Zavala Tsuji et al., 1994	N/A
Rabbit polyclonal αApoI (Genscript)	This paper	N/A
Rat monoclonal αActin (MAC237)	Abcam	Cat#ab50591; RRID: AB_867488
Goat αMouse IgG (H+L) Cross-Adsorbed Secondary Antibody, Alexa Fluor 488	Thermo Fisher Scientific	Cat#R37120; RRID: AB_2556548
Goat αMouse IgG (H+L) Cross-Adsorbed Secondary Antibody, Alexa Fluor 594	Thermo Fisher Scientific	Cat# R37121; RRID: AB_2556549
Donkey αRabbit IgG (H+L) Secondary Antibody, IRDye 800CW	LI-COR Biosciences	Cat#925-32213; RRID: AB_2715510
Goat αRat IgG (H+L) Secondary Antibody, IRDye 680LT	LI-COR Biosciences	Cat#926-68029; RRID: AB_10715073
Bacterial and Virus Strains		
One Shot TOP10 Chemically Competent *Escherichia coli*	Thermo Fisher Scientific	Cat#C404010
NEB Turbo Competent *Escherichia coli*	New England Biolabs	Cat#C2984I
Chemicals, Peptides, and Recombinant Proteins		
Mercurochrome	Sigma-Aldrich	Cat#M7011
ApoI peptide for antibody generation by Genscript FQRDASTKDEKRSGC	This paper	N/A
Ecdysone 22 Oxidase (E22O) His-tagged recombinant protein	This paper	N/A
LD540	Christoph Thiele (Spandl et al., 2009)	N/A
Critical Commercial Assays		
Megascript T7 *in vitro* transcription kit	Thermo Fisher Scientific	Cat#AMB13345
20-hydroxyecdysone enzyme immunoassay (EIA) kit	Cayman Chemical	Cat#501390
Deposited Data		
EcR KD and TL2 KD midgut lipidomics raw data	This paper	Metabolights: MTBLS827
Experimental Models: Cell Lines		
Plasmodium: P. falciparum NF54: wild-type	Carolina Barillas-Mury (Molina-Cruz et al., 2013)	BEI Resources: Cat#MRA-1000
Human: Cryopreserved primary hepatocytes: male, wild-type	BioIVT	Cat#M00995
Human: Fibroblasts: 3T3-J2	H. Green (Rheinwald and Green., 1975)	Kerafast: Cat#EF3003 RRID: CVCL_W667
Human: Embryonic kidney cells: HEK293E	American Type Culture Collection (ATCC)	Cat#CRL-10852 RRID: CVCL_6974
Experimental Models: Organisms/Strains		
Mosquito: *Anopheles gambiae* G3: wild-type	B.E.I. Resources	Cat#MRA-112
Mosquito: *Anopheles gambiae* X1: attP at 2L:10526503	Eric Marois (Volohonsky et al., 2015)	N/A
Mosquito: *Anopheles gambiae* X13: attP at 2L:11322315	Eric Marois (Volohonsky et al., 2015)	N/A
Mosquito: *Anopheles gambiae* VZC: P_{vasa2}::SpCas9; P_{3xPax3}::DsRed	This paper	N/A

(*Continued on next page*)

Continued

REAGENT or RESOURCE	SOURCE	IDENTIFIER
Mosquito: *Anopheles gambiae* gZPG: P_{U6}::Zpg $gRNA_{ab}$; P_{U6}::Zpg $gRNA_c$; P_{3xPax3}::EYFP; P_{vasa2}::EYFP	This paper	N/A
Oligonucleotides		
Primers for qRT-PCR: See Table S2	This paper	N/A
Primers for cloning and dsRNA template production: See Table S4	This paper	N/A
Zpg $gRNA_a$ targeting sequence: GCGGCTTCACTGTCGTGTGA	This paper	N/A
Zpg $gRNA_b$ targeting sequence: CCAAGTGTTTGCATTCCTGG	This paper	N/A
Zpg $gRNA_c$ targeting sequence: GATCCGATCACGCAGTCGAT	This paper	N/A
Recombinant DNA		
pCR2.1 TOPO	Thermo Fisher Scientific	Cat#450641
pCR2.1 EGFP	Baldini et al., 2013	N/A
pCR2.1 EcR	Baldini et al., 2013	N/A
pCR2.1 USP	This paper	N/A
pLL10-Lp	Elena A. Levashina This paper	N/A
pDSAY	Eric Marois Volohonsky et al., 2015	RRID: Addgene Cat#62291
pDSAR	Eric Marois Volohonsky et al., 2015	RRID: Addgene Cat#62292
Transgenesis helper plasmid (pENTR R4-vas2-integrase-R3)	Eric Marois Volohonsky et al., 2015	RRID: Addgene Cat#62299
pDSAY-gZPG	This paper	N/A
pDSAR-VZC	This paper	N/A
PX165 (*Streptococcus pyogenes* Cas9)	Feng Zhang Ran et al., 2013	RRID: Addgene Cat#48137
VR2001-TOPO	Eric Calvo Calvo et al., 2006	N/A
VR2001-Ecdysone 22 Oxidase (E22O)	This paper	N/A
Software and Algorithms		
Broad Institute gRNA design algorithm	Doench et al., 2016	https://portals.broadinstitute.org/gpp/public/analysis-tools/sgrna-design
MIT gRNA design algorithm	Hsu et al., 2013	http://zlab.bio/guide-design-resources
RNA folding algorithm	Hofacker et al., 1994	http://rna.tbi.univie.ac.at/cgi-bin/RNAWebSuite/RNAfold.cgi
Primer-BLAST primer design algorithm	Ye et al., 2012	https://www.ncbi.nlm.nih.gov/tools/primer-blast/index.cgi
MyHits protein sequence motif algorithm	Pagni et al., 2007	https://myhits.isb-sib.ch/cgi-bin/motif_scan
Tracefinder 3.3	Thermo Fisher Scientific	Cat#OPTON-30493
Progenesis QI	Nonlinear dynamics	https://www.nonlinear.com/progenesis/qi/
Prism 7 graphical and statistical software	GraphPad software	https://www.graphpad.com/scientific-software/prism/
JMP Pro 13 graphical and statistical software	SAS Institute	https://www.jmp.com/en_us/software/predictive-analytics-software.html
FIJI (version 1.52a)	Schindelin et al., 2012	https://imagej.nih.gov/ij/index.html
StudioImageLite western blot analysis software	Li-Cor	https://www.licor.com/bio/products/software/image_studio_lite/
Other		

CONTACT FOR REAGENT AND RESOURCE SHARING

Further information and requests for resources and reagents should be directed to and will be fulfilled by the Lead Contact, Flaminia Catteruccia (fcatter@hsph.harvard.edu).

EXPERIMENTAL MODEL AND SUBJECT DETAILS

Rearing of Anopheles gambiae mosquitoes

Anopheles gambiae mosquitoes (wild-type G3 and transgenic strains) were reared in cages at 27°C, 70%–80% humidity on a 12 h light:12 h dark cycle. Adults in colony cages were fed on 10% glucose solution *ad libitum* and weekly on human blood (Research Blood Components, Boston, MA). Males and females were separated as pupae to ensure the virgin status of females. The wild-type G3 has been verified as *A. gambiae* by PCR and DNA sequencing of the amplified products (Santolamazza et al., 2008).

Culturing of Plasmodium falciparum NF54 parasites

P. falciparum (NF54 strain) was cultured as asexual stages between 0.2 and 2% parasitemia at 37°C in human erythrocytes at 5% hematocrit (Interstate Blood Bank, Memphis TN) using RPMI medium 1640 supplemented with 25mM HEPES, 10mg/l hypoxanthine, 0.2% sodium bicarbonate, and 10% heat-inactivated human serum (Interstate Blood Bank) under a gas mixture of 5% O_2, 5% CO_2, balanced N_2 for up to 8 weeks according to established protocols (Trager and Jensen, 1976; Ifediba and Vanderberg, 1981). Gametocytogenesis was induced by raising parasitemia > 4% and incubating cultures for 14–20 days (d) to accumulate stage IV and V male and female gametocytes, with media replaced daily. To inactivate gametocytes and render cultures non-infectious, infectious cultures were heat-exposed at 42°C for 15 min immediately prior to feeding of mosquitoes. This strain has been confirmed to be *P. falciparum* by PCR followed by DNA sequencing of the amplified products (Snounou et al., 1993). The *Plasmodium falciparum* NF54 strain is used under the permissions of a material transfer agreement from the laboratory of Carolina Barillas-Mury, National Institutes of Health, Bethesda, MD, USA.

Culturing of primary human hepatocytes

Cryopreserved male human primary hepatocytes (BioIVT, Westbury, NY) were cultured according to the protocols extensively laid out in (March et al., 2015). Briefly, thawed cells were seeded onto micropatterned collagen islands in well plates and cultured at 37°C, 5% CO_2 using DMEM with L-glutamine medium supplemented with 1% penicillin-streptomycin. These cells were validated by the distributor. After 24 h hepatocyte islands were surrounded by supporting cells from the male mouse fibroblast cell line 3T3-J2 (Rheinwald and Green, 1975) and then co-cultured as above. Fibroblasts were cultured at 37°C, 5% CO_2 using DMEM medium supplemented with 10% bovine serum and 1% penicillin-streptomycin.

METHOD DETAILS

P. falciparum infections of A. gambiae mosquitoes

Cages of female mosquitoes aged 4–7 d were blood fed on ~320 μl *P. falciparum* culture for 30–60 min via heated membrane feeders and introduced into a custom-built glove box (Inert Technology, Amesbury MA). Mosquitoes not fully engorged were removed, and blood-fed mosquitoes were fed 10% glucose solution *ad libitum* until dissection. At dissection time points, mosquitoes were aspirated into 80% ethanol and transferred to 1X phosphate-buffered saline (PBS) (ookinete, oocyst stages) or aspirated into ice-cold PBS or RPMI (sporozoites stages). At least 3 biological replicates of each infection were performed.

Ookinete and early oocyst counts

Mosquitoes were dissected at 24 h (ookinetes) or 48 h (early oocysts) pIBM and any remaining blood meal was removed. Midguts were fixed in 4% formaldehyde for 30–40 min, permeabilized and blocked for 1 h in PBS, 0.1% Triton (PBS-T), 1% bovine serum albumin (BSA) at 22°C, and stained with a mouse α*Pf*s25 monoclonal primary antibody 4B7 (B.E.I Resources, Atlanta, GA) (1/200), followed by an Alexa 488 goat αmouse secondary antibody (Thermo Fisher Scientific, Waltham, MA) (1/400). Immunofluorescently-labeled midguts were mounted in Vectashield with DAPI (Vector Laboratories, Burlingame, CA), imaged at 100X or 200X on a Zeiss Inverted Observer Z1 and parasites counted.

Late oocyst counts and measurements

From 5 d pIBM onward, midguts were stained directly in 2 mM mercurochrome (Sigma-Aldrich, St. Louis, MO) for 12 min, while ovarian development was also scored. The mosquito carcass including ovaries was preserved at 22°C in > 70% ethanol until eggs could be counted later. Mercurochrome-stained midguts were imaged at 100X or 200X on an Olympus Inverted CKX41 microscope, and oocysts were counted and measured using scaled images in FIJI (Schindelin et al., 2012). Burst oocysts were excluded from oocyst size analysis. Mean oocyst size was calculated for each midgut to avoid pseudoreplication.

Sporozoite counts

Mosquitoes were decapitated and the salivary glands of individual females were collected in a small volume of RPMI and disrupted using a handheld disposable pestle. Released sporozoites were spun at 8000 *g* for 10 min at 4°C and resuspended in a known volume

of RPMI. Sporozoites in 0.1 μl were counted using a disposable hemocytometer at 200X or 400X magnification on an Olympus Inverted CKX41 microscope with phase-contrast microscopy. Sporozoite totals for each mosquito were calculated. Median sporozoite totals per oocyst were estimated at the population level using mosquitoes collected on different days following an infectious blood meal on d 1: median sporozoite intensity at d 18 was divided by median oocyst intensity at d 7–8. Data from infections presented in Figures 3 and 5 were pooled for this calculation.

Generation of transgenic mosquito lines

gRNA design

The *zpg* locus (*AGAP006241*) was sequenced to identify SNPs present within our *A. gambiae* strains. gRNA design tools available at the Broad Institute (https://portals.broadinstitute.org/gpp/public/analysis-tools/sgrna-design (Doench et al., 2016)) and the Zhang laboratory, MIT (http://zlab.bio/guide-design-resources (Hsu et al., 2013)) were used to design three gRNAs with minimal off-target sites and mathematically determined optimal cutting. Multiple gRNA sequence targets were chosen to maximize the chances of generating gene knockouts ($gRNA_a$: 5′–GCGGCTTCACTGTCGTGTGA–3′; $gRNA_b$: 5′–CCAAGTGTTTGCATTCCTGG–3′; $gRNA_c$: 5′–GATCCGATCACGCAGTCGAT–3′). gRNAs were synthetized as gBlocks (Integrated DNA Technologies, Skokie, IL) under the control of the $U6_{57}$ promoter (322bp upstream of *AGAP013557*) (Hammond et al., 2016) and followed by a polyT sequence terminator. $gRNA_a$ and $gRNA_b$ were synthesized within a single gBlock as a tethered pair connected by a 21bp sequence (5′–TTCACTGTGCGCATTATATAT–3′) predicted not to interfere with gRNA secondary structure (RNAfold) (Hofacker et al., 1994). $gRNA_c$ was synthesized as a second gBlock.

Plasmid construction

A 2.3 kb fragment of the *vasa2* promoter (Papathanos et al., 2009) was amplified from genomic DNA with primers 5′–CAGGTCT CAATCCCGATGTAGAACGCGAG–3′ and 5′–CGGTCTCACATATTGTTTCCTTTCTTTATTCACCGG–3′. SpCas9 was amplified from plasmid PX165 (Addgene #48137) (Ran et al., 2013) with primers 5′–CAGGTCTCATATGGACTATAAGGACCACGACGGAG–3′ and 5′–CAGGTCTCAAAGCTTACTTTTTCTTTTTTGCCTGGCC–3′. The fragments were cloned via Golden Gate ligation into pDSAR16, a transgenesis plasmid that provides an SV40 terminator, an attB site for ϕC31 transgenesis into attP-containing docking lines, and a 3xPax3-RFP selectable marker (Volohonsky et al., 2015). The two gRNA-containing gBlocks were cloned into the pDSAY transgenesis plasmid (Volohonsky et al., 2015). To enable *in vivo* fluorescence detection of the adult germline, an EYFP reporter under the control of the *vasa2* promoter was included on this transgene. The *vasa2* promoter region was amplified from genomic DNA with primers (5′–CGGTCTCACGCGCGATGTAGAACGCGAGCAAA–3′) and (5′–CAGGTCTCACCATATTGTTTCCTTTCTTTATT CACCGG–3′). The EYFP-SV40 terminator cassette was amplified from pDSAY using primers (5′–CAGGTCTCAATGGTGAG CAAGGGCG–3′) and (5′–CAGGTCTCACGCGGCTTTAAGATACATTGATGAGTTTGGAC–3′). The two fragments were cloned into the AscI site in the pDSAY plasmid via Golden Gate ligation. Completed plasmids were sequenced to verify correct assembly.

Transgenesis

The *zpg* gRNA construct (400 ng/μl) and Cas9 construct (400 ng/μl) were injected into the posterior of freshly-laid embryos from *An. gambiae* X13 (n = 1663) and X1 (n = 2585) attP-containing lines (Volohonsky et al., 2015), respectively, in conjunction with 80 ng/μl of a helper plasmid expressing ϕC31 integrase. Adults surviving injection were crossed to the wild-type G3 strain to identify and isolate transgenic lines gZPG(Zpg) and VZC(Cas9), which were both verified as single insertions by DNA sequencing around the attP insertion sites. These lines were subsequently backcrossed four times to wild-type. Transgenes were made homozygous using the fluorescence intensity of the neuronal Pax marker and true breeding was verified in subsequent generations by the absence of non-fluorescent progeny.

Generation of Δzpg females

Zpg/+ control and Zpg/Cas9 mutant females, hereafter Δ*zpg* mutants, were generated as the F1 progeny of Zpg transgene homozygotes and Cas9/+ heterozygotes. Rare Zpg/+ F1 females with ovarian phenotypes due to the maternal contribution of Cas9 to the egg were excluded from the analysis. To eliminate any bias, rearing and feeding effects in experiments, controls and Δ*zpg* mutants were not separated during larval development or in adulthood by the DsRed fluorescence of the Cas9 transgene until after blood feeding (and, if applicable, *P. falciparum* development) had taken place. Controls and Δ*zpg* mutant females did not differ in wing length size or in their ability to take a blood meal. The ovarian phenotype was scored after dissection or through the cuticle via the *vasa2*-EYFP marker in the Zpg transgene, present in all individuals, under a Leica M80 fluorescence dissecting scope.

Ecdysteroid inactivation using the oxidase E22O

The fungal ecdysteroid-22-oxidase (E22O) from *Metarhizium rileyi* (Kamimura et al., 2012) catalyzes the inactivation of 20E through the oxidation of the hydroxyl group at the carbon backbone position 22. The gene encoding E22O was codon-optimized for mammalian expression and synthesized by BioBasic (Markham, ON, Canada). The E22O construct was engineered to contain the mature protein and a 6X-His tag before the stop codon, subcloned into the VR2001 TOPO vector (a modified version of the VR1020 vector used in Calvo et al., 2006; Vical Incorporated, San Diego CA), and transformed in One Shot TOP10 Chemically Competent *E. coli* (Thermo Fisher Scientific). A total of 1 mg of plasmid DNA (VR2001-E22O construct) was obtained using GeneElute HP endotoxin-free plasmid MEGA prep kit (Sigma-Aldrich). Plasmid DNA was sterilized through a 0.22 μm filter, and recombinant protein was produced by transfecting human embryonic kidney cells (HEK293E; American Type Culture Collection, Manassas, VA). The

cell supernatant was collected 72 h after transfection and loaded onto Nickel-charged HiTrap Chelating HP column (5 mL bed volume; GE Healthcare Life Sciences, Marlborough MA) following the manufacturer's directions. Fractions were step-eluted with 5, 20, 300 and 1000 mM imidazole (in 50 mM Tris, 500 mM NaCl, pH 8.0) and then loaded onto a size-exclusion column (Superdex 200 HR10/30; GE Healthcare Life Sciences) using the ÄKTA purifier system (GE Healthcare Life Sciences). Proteins were eluted isocratically at a flow rate of 0.5 ml/min in 50 mM Tris, 150 mM NaCl, pH 8.0. Purified E22O was separated in a 4%–12% Bis-Tris NuPAGE Gel (Thermo Fisher Scientific) and visualized by Coomassie stain. Protein identity was verified by automated Edman degradation at the Research Technologies Branch, NIAID, NIH. The catalytic activity of recombinant E22O was determined as described in Kamimura et al. (2012). A total of 69 nL (Figure S2C) or 138 nL (Figure 2, Figure S2B) of purified protein (0.5 mg/ml) was injected into wild-type females 4–5 d after eclosion, and 3–6 h prior to feeding on a *P. falciparum*-infected blood meal. Control females were injected with an equal volume and concentration of BSA (66 kDa), which has a comparable molecular mass to E22O (76 kDa). Females were randomly assigned to injection groups and surviving females were used in experiments.

Measurement of ecdysteroid levels

Control or Δ*zpg* mutant females and E22O- or BSA-injected females were blood fed on human blood and then anaesthetized on ice at 26 h or 36 h pBM as required. Egg development was scored in Δ*zpg* mutant females through the cuticle by the expression of a *vasa2*-EYFP transgene to preserve circulating ecdysteroids in the hemolymph within the body. Heads were removed from females and carcasses were stored in pairs at −80°C in 80 μl of 100% methanol. Ecdysteroid levels were determined using the 20E enzyme immunoassay (EIA) kit (Cayman Chemical, Ann Arbor, MI), following the recommended protocol. Each sample was measured in duplicate. This assay detects 20E but according to the manufacturer, also cross reacts with ecdysone, 2-deoxy-20-hydroxyecdysone, and 2-deoxy-edysone, hence we assayed ecdysteroid levels. EIA plates were read on a spectrophotometer at 412 nm after 90 min.

Gene expression knockdown using dsRNA

Creation of templates for dsRNA production

PCR fragments of *EcR* (*AGAP028634*; 435 bp) and the eGFP control (495 bp) were amplified from plasmids pCR2.1-EcR and pCR2.1-eGFP described previously (Baldini et al., 2013). A 481 bp fragment of *USP* (*AGAP002095*) was amplified from cDNA prepared from female whole bodies minus head using USP-FWD: 5′–GGAAGCAATGGAGGTGGAG–3′ and USP-REV: 5′–CATAGAATTCTGGC CAACGC–3′, and then cloned into the pCR2.1 construct (Thermo Fisher Scientific). A 600 bp fragment of *Lp* (*AGAP001826*) corresponding to bases 9452–10051 of the *Lp* cDNA was amplified from plasmid pLL10-Lp, a gift from Miranda Whitten and Elena A. Levashina (Max Planck Institute for Infection Biology, Berlin), using a primer matching the inverted T7 promoters: 5′–TAATACGACT CACTATAGGG–3′. Purified constructs were recovered from NEB Turbo chemically-competent *E. coli* (New England Biolabs, Ipswich, MA) and verified by DNA sequencing prior to use. Amplifications from pCR2.1-based vectors used universal primers against the vector backbone to add the T7 promoter (lowercase) to both ends: pCR2.1-T7F: 5′–taatacgactcactatagggCCGCCAGTGTGCTG GAA–3′ pCR2.1-T7R: 5′–taatacgactcactatagggGGATATCTGCAGAATTCGCCC–3′. PCR fragments of *TEP1* (*AGAP010815*; 395 bp) and *TL2* (*AGAP000211*; 406 bp) were amplified directly from cDNA prepared from female whole bodies minus head using the following primers: TEP1-FWD: 5′–taatacgactcactatagggTTTGTGGGGCTGAAAGCGCTG–3′, TEP1-REV: 5′–taatacgactcactatagggACCACGTAACCGCTCGGTAAG–3′, based on Jaramillo-Gutierrez et al. (2009); TL2–FWD: 5′–taatacgactcactatagggCTTTAGT CGGGTGGAGGACA–3′, TL2–REV: 5′–taatacgactcactatagggGATGATCGGTGTTCGGCTT–3′. PCR product sizes and yield were confirmed by gel electrophoresis. dsRNA was transcribed and purified from the PCR templates using the Megascript T7 transcription kit (Thermo Fisher Scientific) as described previously (Blandin et al., 2004; Rogers et al., 2009).

dsRNA injections

For *GFP, EcR, USP, TEP1, Lp* and *TL2* single knockdown experiments, 690 ng of dsRNA (ds*GFP*, ds*EcR,* ds*USP,* ds*TEP1*, ds*Lp,* ds*TL2*) was injected (Nanoject II, Drummond) at a concentration of 10 ng/nl into adult females within 1 d of eclosion. In double knockdown groups, dsRNAs were mixed 1:1 and injected in twice the volume (1.38 μg). Females were randomly assigned to injection groups and surviving females were used in subsequent experiments. Gene knockdown levels were determined in at least 3 biological replicates by quantitative real-time PCR at 2 d post injection (Figure S7).

RNA extraction, cDNA synthesis and qRT-PCR

Female mosquitoes (n = 5–10) were decapitated in PBS and transferred to TRI reagent (Thermo Fisher Scientific). Samples were stored at −80°C and RNA was extracted according to the manufacturer's instructions, with a modification to wash the pelleted RNA with 70% ethanol in RNase-free water three times. RNA was DNase treated using Turbo DNase (Thermo Fisher Scientific) and quantified using a NanoDrop Spectrophotometer 2000c (Thermo Fisher Scientific). cDNA synthesis was performed as in Rogers et al. (2008). Approximately 2 μg of RNA was used in 100 μl cDNA reactions. Primers (Integrated DNA Technologies) used for quantitative real-time PCR (qRT-PCR) (Table S2) were previously published or designed using Primer-BLAST (Ye et al., 2012) where possible over exon-exon junctions or in separate exons and checked for potential off-target binding. cDNA samples from 3 biological replicates were diluted 10-fold for qRT-PCR. Quantification was performed in duplicate 15 μl reactions, containing 1X Fast SYBR Green Master mix for qRT-PCR (Thermo Fisher Scientific), primers and 5 μl of diluted cDNA. Reactions were run on a StepOnePlus qRT-PCR thermocycler (Thermo Fisher Scientific). Relative quantities were determined using a standard curve and normalized

against the ribosomal gene *RpL19* (*AGAP004422*), which does not change significantly with blood feeding (Marinotti et al., 2006). To determine the expression of additional TAG lipases, we assayed transcripts of *AGAP000210*, *AGAP001764* and *AGAP007672*. Amplifications using 4 different primers sets designed against transcripts of *AGAP001764* were attempted but were not successful, and no RNA sequencing reads were detected in mixed sex adults from this gene model (Gibbons et al., 2009). We concluded that this gene is a pseudogene.

Sporozoite gliding and infectivity assays

P. falciparum sporozoites from salivary glands of ds*GFP* and ds*EcR* females at 12 d and 18 d pIBM were assessed for their ability to glide on coated plates, invade, and infect micropatterned human primary hepatocytes in 96-well plate format assays according to protocols described in March et al. (2015). To assay sporozoite gliding ability, 7000 sporozoites were added per well of a 96-well plate coated with 5 μg/ml of a mouse α*Pf*CSP monoclonal primary antibody 2A10 (B.E.I Resources). Plates were spun down at 3000 rpm for 5 min, and were incubated at 37°C for 45 min. Following incubation, plates were fixed and CSP trails were stained as in March et al. (2015).

For invasion and infection assays, 10000 and 100000 sporozoites, respectively, from each group, were added per well of a 96-well plate containing micropatterned human primary hepatocytes. Plates were spun down at 3000 rpm for 5 min, then incubated at 37°C. For the invasion assay, plates were fixed in 4% paraformaldehyde (PFA) at 3 h post-invasion. Cells were double-stained with α*Pf*CSP to label both intracellular and extracellular parasites, and 3 wells were counted per condition, with a minimum of 100 events scored per well. For the infection assays, plates were fixed in 100% MeOH at 2 d post-invasion. Cells were stained with mouse α*Pf*HSP70 monoclonal primary antibody 4C9 (Tsuji et al., 1994), following the protocol described in March et al. (2015).

Western blotting

Abdominal fat body (n = 8) was dissected from 4-d-old blood-fed females at 24 h and 48 h pBM in cold PBS and frozen at −80°C in modified breaking buffer (Hansen et al., 2005) (50 mM Tris, pH 8.0; 1% NP40; 0.25% sodium deoxycholate; 150 mM NaCl; 1 mM EDTA; 1X protease inhibitor mixture (Roche, Basel, Switzerland)). Samples were homogenized, and the insoluble material removed by centrifugation at 20000 *g* at 4°C. Protein was quantified using a Quick Start Bradford assay (Bio-Rad, Hercules, CA). 30 μg of soluble protein was denatured and run in parallel between 3%–8% Tris-Acetate NuPAGE and 4%–12% Bis-Tris NuPAGE gels (Thermo Fisher Scientific) due to the large size difference between ApoI (288 kDa) and the actin loading control (42 kDa). Protein was transferred to PVDF membranes using an iBLOT2 transfer system (Thermo Fisher Scientific), and membranes were washed twice in 1X PBS-T, then blocked for 30 min at 22°C in Odyssey Blocking Buffer (Li-Cor, Lincoln, NE). Membranes from 3%–8% gels were incubated with rabbit αApoI (1:4000) polyclonal primary antibody and those from 4%–12% gels were incubated with rat αActin monoclonal primary antibody MAC237 (Abcam, Cambridge, UK) (1:5000), both shaking overnight at 4°C. Affinity-purified antibodies targeting the large ApoI subunit of Lp were generated by Genscript (Piscataway, NJ) using the peptide FQRDASTKDEKRSGC conjugated to a carrier protein. Following the primary antibody, membranes were washed with PBS-T, and incubated with secondary antibodies (donkey αrabbit 800CW and goat αrat 680LT (Li-Cor), both at 1:20,000) in blocking buffer with 0.01% SDS for 1 h at 22°C. Membranes were washed thoroughly with PBS-T before imaging with the Odyssey CLx scanner. Images and band intensities were analyzed in StudioImageLite (Li-Cor).

Staining of neutral lipids with LD540

Midguts (n = 10) were dissected from ds*GFP*- or ds*TL2*-injected females at 48 h pBM and fixed with 4% PFA for 45 min at 22°C, and then neutral lipids were stained with LD540 in PBS (0.5 μg/ml) for 5 min at 22°C according to Spandl et al. (2009). Nuclei were stained with DAPI for 5 min before mounting with Vectashield (Vector Laboratories). Images were captured at 400X on a Zeiss Inverted Observer Z1.

Lipidomics of mosquito tissues

Midguts from ds*GFP*, ds*EcR*, or ds*TL2* females were collected in pools of 4–5 into 100 μl of isopropanol (HPLC Grade; Honeywell) at 24 h and 48 h pBM, in 3 biological replicates for ds*EcR* or 4 replicates in ds*TL2* analyses. Analyses of polar and non-polar lipids were conducted using an LC-MS system comprised of a Shimadzu Nexera X2 U-HPLC (Shimadzu Corp, Marlborough, MA) coupled to an Exactive Plus orbitrap mass spectrometer (Thermo Fisher Scientific). Tissues were homogenized in a TissueLyser (QIAGEN, Hilden, Germany) with 2, 3mm tungsten beads for 4 min at 20 Hz. Lipids were extracted from tissue homogenates (10 μL) using 190 μL of isopropanol (HPLC Grade; Honeywell) containing 1,2-didodecanoyl-sn-glycero-3-phosphocholine (Avanti Polar Lipids, Alabaster, AL). Lipid extracts were then injected onto an ACQUITY BEH C8 column (100 × 2.1 mm, 1.7 μm; Waters, Milford, MA) and the column was eluted isocratically with 80% mobile phase A (95:5:0.1 vol/vol/vol 10 mM ammonium acetate/methanol/formic acid) for 1 min followed by a linear gradient to 80% mobile-phase B (99.9:0.1 vol/vol methanol/formic acid) over 2 min, a linear gradient to 100% mobile phase B over 7 min, then 3 min at 100% mobile-phase B. Mass spectrometry data was acquired using electrospray ionization in the positive ion mode over 200–1100 *m/z* and at 70,000 resolution. Raw data were processed using TraceFinder 3.3 (Thermo Fisher Scientific) and Progenesis QI (Nonlinear Dynamics, Newcastle upon Tyne, UK) software for detection and integration of LC-MS peaks. Lipid identities were determined based on comparison to reference standards and reference plasma extracts and denoted by total number of carbons in the lipid acyl chain(s) and total number of double bonds in the lipid acyl chain(s).

QUANTIFICATION AND STATISTICAL ANALYSIS

See figure legends for details of the statistical methods used in each experiment. Data was analyzed in GraphPad Prism 7 and JMP Pro 13. Normality was determined using the D'Agostino-Pearson omnibus normality test, using a significance cut-off value of $p = 0.05$. Transformations to generate normally distributed data were attempted prior to statistical testing using parametric methods, and, if unsuccessful, non-parametric statistical methods were used. A significance cut-off value of $p = 0.05$ was used for statistical tests and, where multiple tests were performed, the significance was corrected using a 5% false discovery rate (FDR), or Dunn's multiple comparison correction. Where *P. falciparum* infection intensity was variable between biological replicates, or data were collected over time, Generalized Linear models (GLM) or Standard Least-squares models incorporating replicate, treatment, and time as factors were constructed, with interactions between factors excluded if they were not significant (see Table S3 for full details). Unless indicated, horizontal bars on graphs represent medians. Trendlines illustrate the overall shape of correlations using linear regression but non-parametric statistical methods were used to analyze the data. Proportional data for infection prevalence was compared using a chi-square test where $n > 5$ in all groups, or else using Fisher's Exact test. Wing length, measured in millimeters from the proximal wing notch to the distal tip of the third cross vein, was cubed and used to normalize oocyst and egg count data for mosquito size.

DATA AND SOFTWARE AVAILABILITY

The accession number for the lipidomics data reported in this paper is Metabolights: MTBLS827.

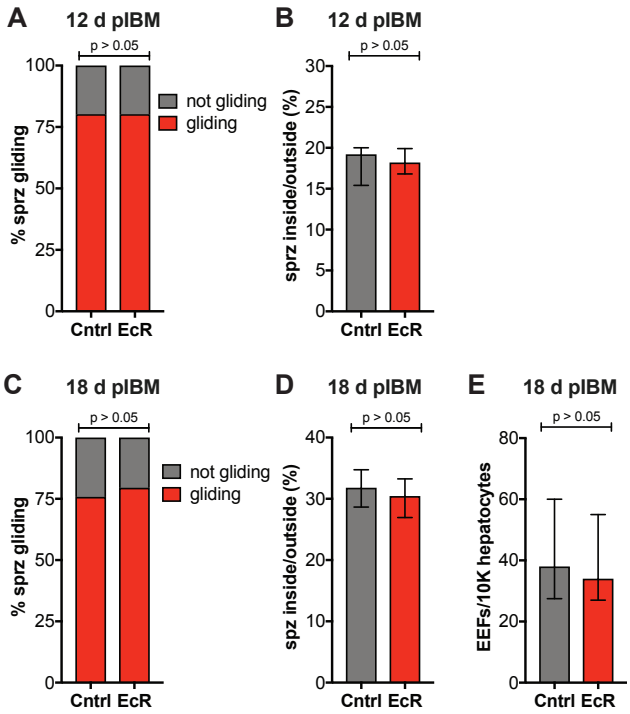

Figure S1. Sporozoite Gliding and Infectivity to Hepatocytes, Related to Figure 5

(A–B) Sporozoites collected from the salivary glands of ds*EcR* (EcR) and ds*GFP* (Cntrl) females at 12 days (d) pIBM display no significant difference in (A) gliding activity (means, Fisher's Exact) or (B) hepatocyte invasion (medians ± IQR, Mann-Whitney), as determined through microscopy by identification of circumsporozoite surface protein (CSP) trails and percent sporozoites inside versus outside hepatocyte cells, respectively.

(C–E) Similarly, sporozoites collected from the same groups at 18 d pIBM show no difference in their (C) gliding activity (means, Fisher's Exact), (D) hepatocyte invasion (medians ± IQR, Mann-Whitney) and (E) development into exoerythrocytic forms (EEFs) (medians ± IQR, unpaired t test).

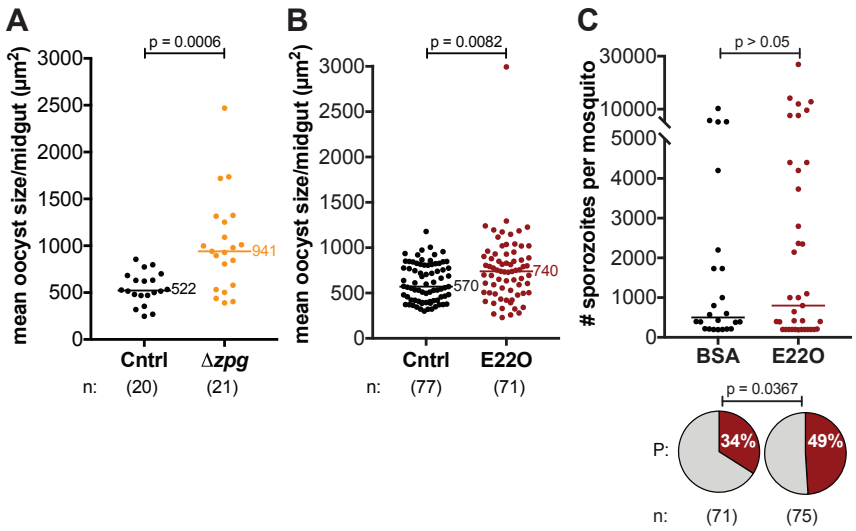

Figure S2. Parasites Grow Faster in Δ*zpg* Mutant and E22O-Injected Females, Related to Figure 5

(A–B) At 8 d pIBM, mean oocyst area is significantly greater in (A) Δ*zpg* females (unpaired t test, Welch's correction) and (B) E22O-injected females (Mann-Whitney) compared to their respective controls (Cntrl).

(C) Salivary glands of E22O-injected females show a higher prevalence of sporozoites at 11–12 d pIBM (Nominal Logistic Regression). There was no difference in intensity (Mann-Whitney). In all panels, n corresponds to the sample size. P = prevalence of infection.

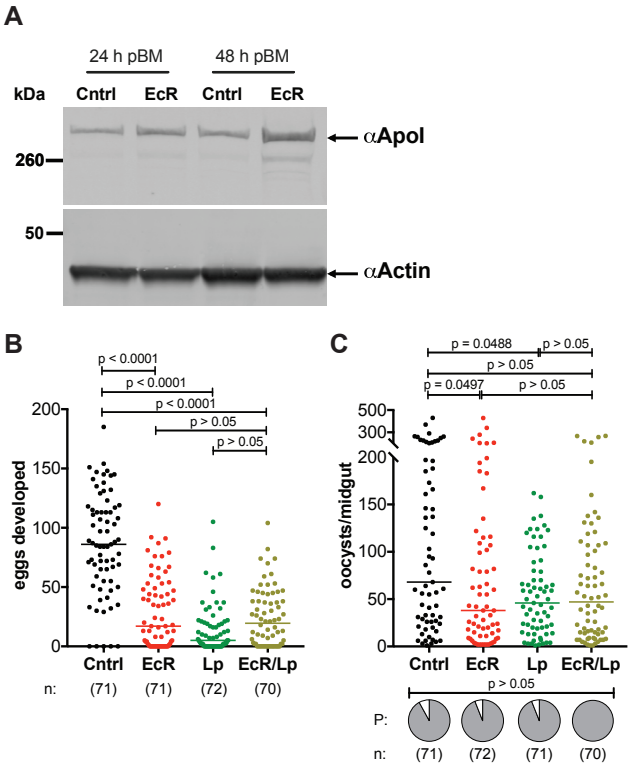

Figure S3. Lp Accumulates in *EcR*-Depleted Females, and Its Silencing Reduces Both Egg and Parasite Numbers, Related to Figure 6

(A) Apol protein (αApol) accumulates in the fat bodies of ds*EcR* females (EcR) pIBM, with a more pronounced effect at 48 h pIBM. Actin (αActin) = loading control. (B and C) ds*EcR*-, ds*Lp*- (Lp), and ds*EcR*/*Lp*- (EcR/Lp) injected females (B) produce fewer eggs (Kruskal-Wallis & Dunn's correction) and (C) have fewer oocysts at 8 d pIBM compared to ds*GFP*-injected controls (Cntrl) (Kruskal-Wallis & Dunn's correction). There is no effect on infection prevalence (Fisher's Exact) (P = prevalence of infection). In all panels where applicable, n corresponds to the sample size.

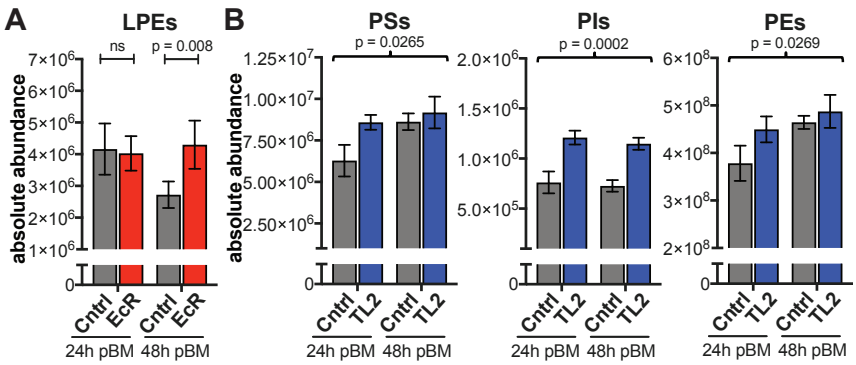

Figure S4. Minor Lipid Species Enriched in ds*EcR* and ds*TL2* Midguts, Related to Figures 6 and 7

(A) ds*EcR*-injected midguts (EcR) have elevated levels of LPEs compared to ds*GFP* controls (Cntrl) at 48 h pBM (means ± SEM, Standard Least-squares model; $p > 0.05$ at 24 h pBM).

(B) ds*TL2*-injected midguts (TL2) are enriched for three additional lipid species: phosphatidylserines (PSs), phosphatidylinositols (PIs), and phosphatidylethanolamines (PEs) (means ± SEM, Standard Least-squares model). See also Table S3.

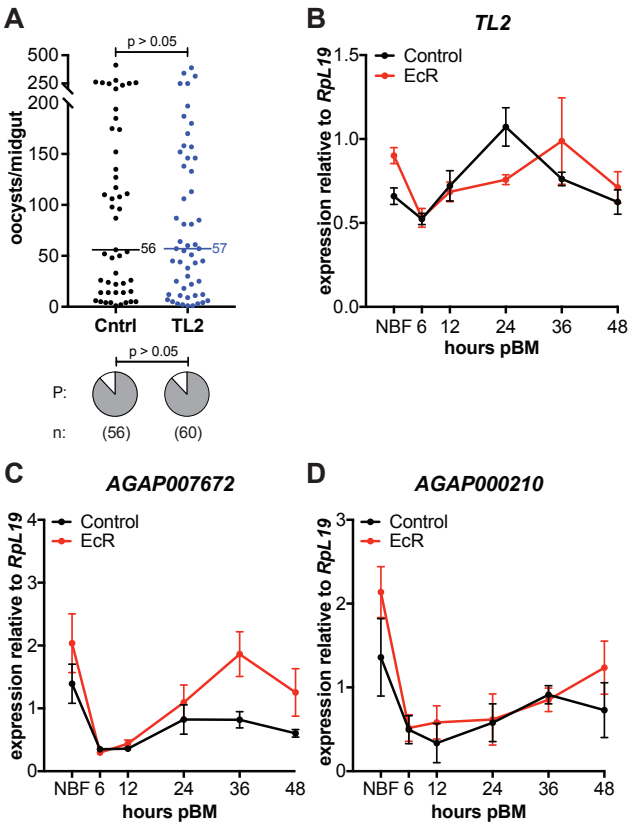

Figure S5. TL2 Does Not Affect Oocyst Numbers, and EcR Does Not Transcriptionally Regulate TAG Lipases, Related to Figure 7

(A) ds*TL2*-injected females (TL2) infected with *P. falciparum* develop the same number of midgut oocysts by 7–8 d pIBM compared to ds*GFP* controls (Cntrl) (Mann-Whitney). There is also no difference in infection prevalence (chi-square) (n corresponds to the sample size; P corresponds to prevalence of infection). (B–D) Expression of neither (B) *TL2*, (C) *AGAP007672*, nor (D) *AGAP000210* was significantly different in ds*EcR* females (EcR) at any time point pBM (means ± SEM, unpaired t tests, FDR corrected; for all time points, $p > 0.05$). NBF = non-blood fed.

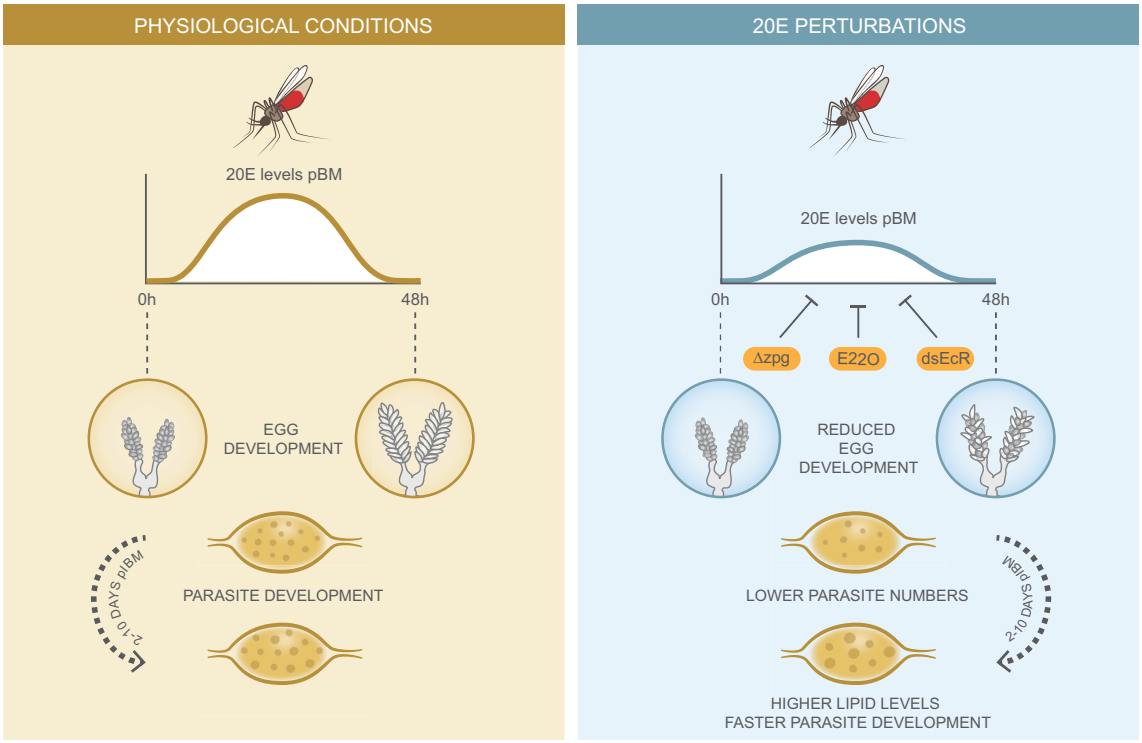

Figure S6. Summary Scheme of Experiments and Findings, Related to Figures 1, 2, 3, 4, 5, 6, and 7

Egg development (top, 0–48 h) and parasite development (bottom, 2–10 d) are represented schematically in physiological conditions (left) and following different manipulations of 20E signaling (right). These manipulations lower 20E levels (Δ*zpg*, E22O) or impair 20E signaling (ds*EcR*) after blood feeding, reduce egg and parasite numbers, and cause a lipid-mediated increase in parasite growth.

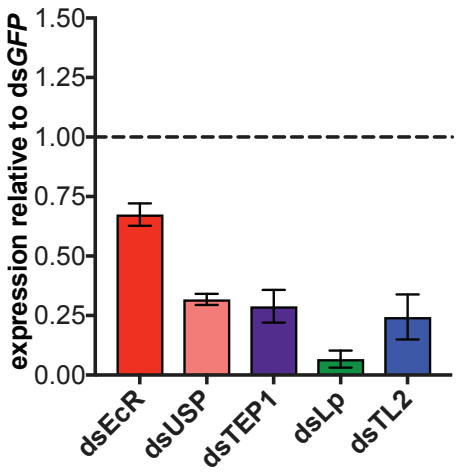

Figure S7. Silencing Efficiencies for dsRNA Injections, Related to Figures 3, 4, 5, 6, and 7

Using qRT-PCR, target gene expression was normalized to expression of the housekeeping ribosomal gene *Rpl19*, and then silencing efficiency was calculated as expression in the treatment group relative to expression in control, ds*GFP*, females (means ± SEM). ds*EcR*: 0.67 *EcR* expression relative to controls (33% knock down). ds*USP*: 0.32 *USP* expression relative to controls (68% knock down). ds*TEP1*: 0.29 *TEP1* expression relative to controls (71% knock down). ds*Lp*: 0.07 *Lp* expression relative to controls (93% knock down). ds*TL2*: 0.24 *TL2* expression relative to controls (76% knock down). See also Table S2.